UNIVERSITY OF CALIFORNIA, MERCED

# Electron-Phonon Coupling in CdSe Nanocrystals

A Thesis submitted in partial satisfaction of the
requirements for the degree of

Master of Science

in

Chemistry and Chemical Biology

by

Joshua Allen Baker

Committee in charge:

Professor David F. Kelley, Chair
Professor Anne Myers Kelley, Advisor
Assistant Professor Erik Menke
Assistant Professor Michael Scheibner

2014

The Thesis of Joshua Allen Baker is approved, and it is acceptable in quality and form for publication on microfilm and electronically:

Anne Myers Kelley

Erik Menke

Michael Scheibner

David F. Kelley, Chair

University of California, Merced

2014

## Dedication

I'd like to dedicate this Thesis work to my beautiful and supportive wife, Maria, and my very supportive parents, David and Kathy. With all your love, teachings, and support, I've become the man I am today and this work would not have been completed without you. Thank you for all that you have done.

Table of Contents

## List of Tables

## List of Figures

## Acknowledgements

I'd like to thank the Chemistry and Chemical Biology group at the University of California, Merced, for the opportunity to further my education and allowing me to obtain a deeper understanding of Chemistry.

I'd like to thank my esteemed committee members, Dr. Anne Myers Kelley, Dr. David Kelley, Dr. Erik Menke, and Dr. Michael Scheibner for your time and insights.

I'd like to also thank my former and current graduate group members whom I have had the pleasure of working with and who have helped me to understanding the vast amount of material and different aspects of nanocrystals including: Dr. Zhong-Jie Jiang, Dr. Xaichen Cai, Dr. Damon Wheeler, Dr. Chen Lin, Dr. Quanqin Dai, Dr. Gary Beane, Cory Sobotta, Youhong Zeng, and Ke Gong.

Additionally I'd like to thank other chemistry group members that I've had the chance to get to know and occasionally talk about ideas: Dr. Jason Hein, Luke Reed, Matt Berry, Ivy Price, Diana Yu, and Blessing Cao.

Lastly I'd like to thank the funding agencies that made all of this possible: the University of California, Merced and the National Science Foundation (NSF) Grant No. CHE-1112192.

Thank you all for making this a memorable experience.

## Abstract

Electron-Phonon Coupling in CdSe Nanocrystals

by

Joshua Allen Baker

Master of Science in Chemistry and Chemical Biology
University of California, Merced, 2014
Professor David F. Kelley, Committee Chair

A size dependent study of electron-phonon coupling of organically capped, wurtzite form CdSe nanocrystals dissolved in chloroform was performed using resonance Raman excitation profiles for the longitudinal optical (LO) phonon fundamental and its first overtone. CdSe nanocrystals with diameters of 2.8, 3.0, 3.2, and 5.2 nm were synthesized from variations of literature procedures and then ligand exchanged with hexadecanethiol ligands to quench the underlying fluorescence in our Raman measurements. The absolute differential Raman cross section for the fundamental is much larger when excited on the high-frequency side of the first absorption maximum whereas cross sections at shorter wavelength excitations were much smaller despite the absorption being much higher at shorter wavelengths. The optical absorption spectrum, the resonance Raman excitation profiles, and depolarization dispersion curves were reproduced using a model for the energies, oscillator strengths, electron-phonon couplings, and dephasing rates of the multiple low lying electronic excitations for each sized nanocrystals.

The electron-phonon coupling for the LO phonon, expressed through the Huang-Rhys parameter, was determined to be in the range of S=0.04-0.15 while a good fit could be obtained using the same value, S=0.08, for the lowest excitonic transition for each particle size. This result shows that there is no size dependence of the electron-phonon coupling strength of the first excitonic transitions for various sized CdSe nanocrystals. Each sized nanocrystal also showed similar features in the higher energy spectral region, 2000-5000 $cm^{-1}$ above the first absorption maximum. This region, typically labeled as the $1P_{3/2}$-$1P_e$ transition, is actually a combination of at least two contributions that vary greatly in their magnitude of electron-phonon coupling strength.

## Introduction and Background

Semiconductor nanocrystals such as CdSe have been intensely studied due to their unique photophysical properties and are of major interest thanks to their implementation across a wide host of applications including solar energy conversion, LEDs, and diode lasers, among others.[1,2] These materials are unique in that they are quantum confined (they display a profound size effect upon being made increasingly small); hence they are also termed quantum dots. Quantum confinement occurs when the size of the nanocrystal becomes comparable to or smaller than the exciton Bohr radius. As the size of the semiconductor nanocrystal becomes smaller, the electronic absorption and photoluminescence spectra shift to lower wavelengths (blue shift), increasing the energy gap, the energy between the valence and conduction bands, within the nanocrystals (Figure 1). This can be accounted for using a particle-in-a-sphere model given as:

$$E_{g,effective}(R) = E_g(\infty) + \frac{\hbar^2 \pi^2}{2R^2}\left(\frac{1}{m_e} + \frac{1}{m_h}\right) - \frac{1.8\,e^2}{4\pi\varepsilon_0 \varepsilon R} \quad (1)$$

where $E_g(\infty)$ is the bulk band gap, $m_e$ and $m_h$ are the effective masses of the electron and hole, and $\varepsilon$ and $\varepsilon_0$ are the relative permittivity of the semiconductor and the permittivity of free space respectively.[2,3] The second term in this equation shows that the effective band gap is inversely proportional to the radius squared, hence an increase in the band gap as the nanocrystal size decreases. The third term, however, due to the Coulomb attraction between the electron and hole, is merely proportional to the inverse of the radius which results in a decrease in band gap as the nanocrystal size decreases. The net effect between these two terms however is dominated by the $1/R^2$ dependence in the second term and thus, the effective band gap increases as the nanocrystal becomes smaller.

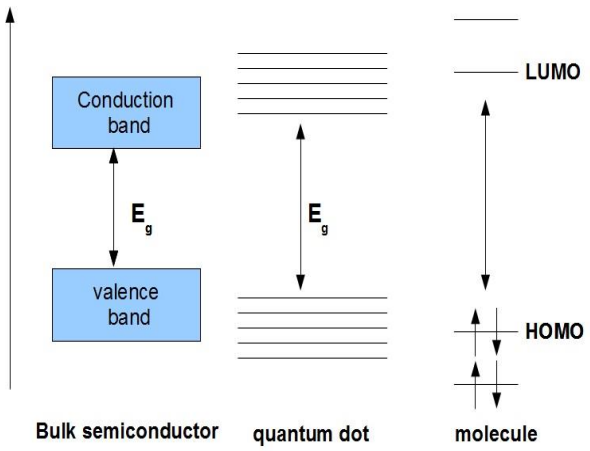


*Figure 1. General diagram of energy levels where the bulk semiconductor has bands of continuous energy levels, quantum dots energy levels become discrete similar to molecules' HOMO-LUMO gap .[4]*

As was alluded to, quantum confinement occurs when the size of the nanocrystal becomes comparable to the Bohr radius. To calculate the size at which noticeable quantum confinement effects begin, the Bohr radius for a nanocrystal can be determined by:

$$\alpha_B = \frac{\varepsilon_0 \varepsilon h^2}{\pi \mu e^2} \quad (2)$$

where $\varepsilon$ and $\varepsilon_0$ are the relative permittivity of the semiconductor and the permittivity of the free space, respectively, $\mu$ is the reduced mass for the electron and hole, given as $\mu = m_e m_h/(m_e+m_h)$, and $e$ is the electric charge.[3] As CdSe is the focus of this study, we take $\varepsilon$ to be 9.7, $\mu$ to be $9.2 \times 10^{-32}$ kg, and arrive at an exciton Bohr radius of approximately 5.7 nm, in good agreement with literature values.[3,5]

Synthetic methods allow one to tune the electrical properties especially when quantum confinement effects dominate for very small nanocrystals, which are commonly referred to as being in the "strong confinement" regime. This is accomplished through careful synthetic control of the overall QD size and shape.[6] As such, quantum confinement effects allow one to model the nanocrystal energy levels and wavefunctions. Optical excitations in CdSe nanocrystals are typically modeled using the effective mass approximation envelope function method.[7] At the unit cell level, the excitation is described as moving an electron from the Se *4p* orbitals to the Cd *5s* orbitals. The electron now resides in the conduction band and the positive region left behind in the valence band is termed a hole. This combination is typically referred to as an electron hole pair or an exciton. The electron and hole wavefunctions are then constructed as products of these unit cell Bloch functions with spherical symmetry envelope functions that give the contributions of each unit cell to the overall wavefunction.

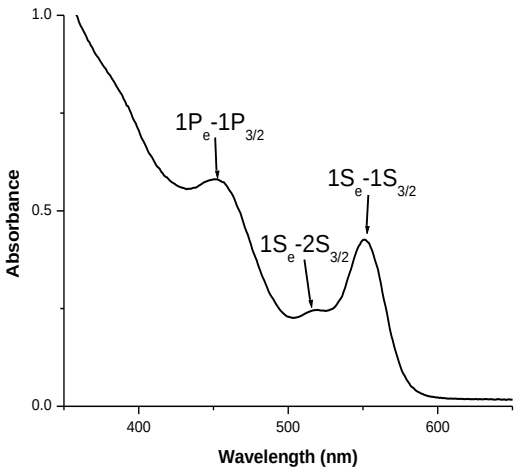


*Figure 2. Linear absorption spectrum of CdSe with typical effective mass approximation assignments*

Experimental absorption spectra of high-quality samples exhibit a fairly sharp lowest energy transition assigned as the $1S_e$-$1S_{3/2}$ in the effective mass approximation envelope function notation (Figure 2). Here, the $1S_e$ stands for the lowest energy state of the electron where the total angular momentum is always taken to be ½ due to the spin ½ of the electron and l = 0 angular momentum of the Cd *s* orbital. The $1S_{3/2}$ is the lowest energy state of the hole, where the subscript 3/2 is the total angular momentum j, which arises from spin-orbit coupling between for the spin ½ of the hole and the l = 1 angular momentum of the Se *p* orbital.[5] Beyond the first exciton, the higher energy region of the absorption spectra only contains a few weakly resolved peaks that appear to be superimposed on a diffuse background that continues to rise with increasing energy. The assignments that are typically given to the higher energy region are shown in Figure 2, however it seems fairly clear that at least part of the background must come from multiple overlapping transitions, each broadened through both homogeneous (natural broadening) and inhomogeneous (polydispersity in size or shape) pathways.

Analysis of CdSe requires one to account for its fine structure for each electronic transition, adding more complexity to our understanding. Crystal field splitting by the wurtzite lattice and electron-hole exchange interaction split the lowest-energy transition into five different energy levels, two of them z-polarized ($0^U$ and $0^L$) and three xy-polarized that are doubly degenerate ($\pm1^U$, $\pm1^L$, and $\pm2^L$) (Figure 3). One z-polarized and two of the xy-transitions are optically allowed ($0^U$, $\pm1^U$, and $\pm1^L$), with the xy-transitions having a total oscillator strength twice that of the z-polarized transition. Additionally for spherical CdSe nanocrystals, the xy-polarized transitions, $\pm1^U$ and $\pm1^L$, lie lower in energy than the z-polarized transition, $0^U$. [28-32]

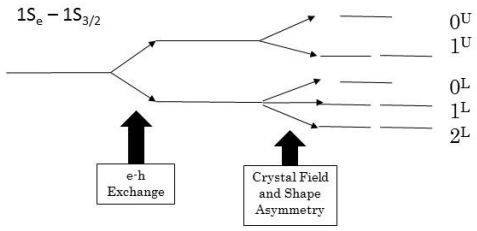


*Figure 3. CdSe fine structure for the first excitonic transition.[2,28]*

One technique that has seemed to be underutilized in the effort to sort out the CdSe electronic structure is that of resonance Raman excitation profile analysis. Measuring and modeling both the absorption and the profiles for multiple Raman transitions can be used to estimate oscillator strengths, positions of contributing transitions, electron-

phonon couplings, and electronic spectral broadening mechanisms.[8-10] Studies have been completed using Raman spectroscopy to probe the ground-state structure of semiconductor nanocrystals and measurements of resonance Raman overtone to fundamental ratios have been used to measure electron-phonon coupling strengths[11-14], however the only excitation profile analysis in CdSe nanocrystals that we are aware of was carried out more than 20 years ago by the Alivisatos group. They measured relative Raman excitation profiles and depolarization dispersion curves, but did not try to put the intensities on an absolute scale nor did they attempt to explain the profiles quantitatively.[15-17]

The electronic properties of semiconducting materials are influenced by the position of their nuclei. When excited, the nuclei in crystals undergo vibrational motions known as "phonons." Our research project studies CdSe nanocrystals (NCs), which have a longitudinal optical (LO) phonon at approximately 206 $cm^{-1}$.[18] The LO phonon is the highest frequency optical phonon that is the dominant feature in a Raman spectrum. One can visualize the LO phonon in a 1-dimensional diatomic crystal where the Cd and Se ions vibrate relative to one another within the unit cell. Each unit cell then undergoes the same motion and this motion is repeated throughout the crystal lattice (Figure 4). This can ultimately be extended to 3-dimensions, however visualizing the vibration within CdSe's wurtzite or zincblende unit cell is difficult. Other phonon modes of CdSe NCs include the transverse optical modes at slightly lower frequencies and acoustic phonons at even lower frequencies, however all of these are much weaker and are not usually observed in a room temperature Raman spectrum.

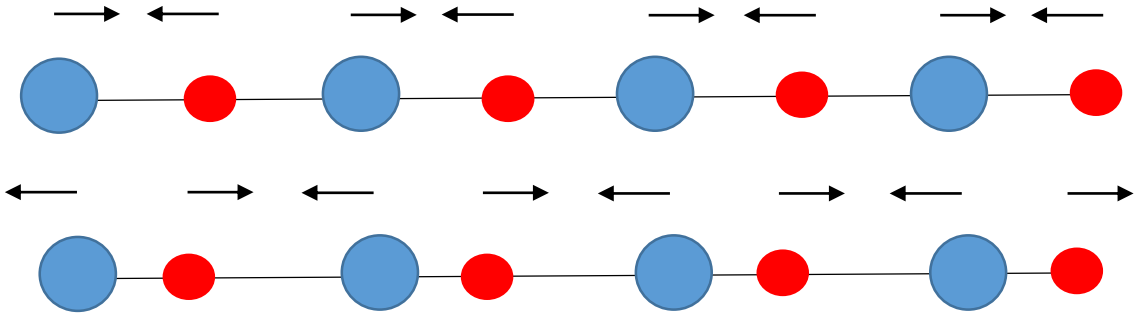

*Figure 4. Graphical representation of the longitudinal optical phonon of a 1-dimensional diatomic lattice where Cd and Se atoms in each unit cell vibrate relative to each other and is repeated throughout the entire lattice.*

Electron-phonon coupling (EPC) refers to the coupling between electronic excitations and nuclear vibrations.[1] Excitations distort the position of the nuclei relative to one another and change the energy gap of the electronic states and therefore regulate electronic relaxation processes. The creation of an exciton, or electron-hole pair, can induce nuclear motion by changing the nuclear position from that of the ground state.

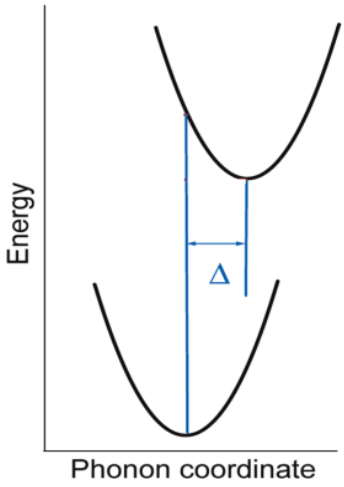


*Figure 5. Electron-phonon coupling in terms of the normal coordinate of the phonon mode.[2]*

The magnitude of EPC is typically reported in the literature through the Huang-Rhys factor, *S*. The Huang-Rhys factor is determined by

$$S = \frac{\Delta^2}{2} \tag{3}$$

where $\Delta$ is the displacement between the ground and excited state potential minima along a phonon coordinate (Figure 5).[1] Studying the magnitude of EPC can be useful in understanding fundamental and technological influences including: (i) carrier multiplication, where one high energy photon produces multiple electron-hole pairs; (ii) in interfacial charge separation, which is the transfer of an electron or hole from a SC NC to a surface mode or across a heterojunction between two different semiconductor materials; (iii) other processes that depend on the time scales for dissipation of the excess energy of charge carriers.[19]

EPC in CdSe nanocrystals has been experimentally and theoretically determined and reported throughout the literature.[1,3] However, values of *S* for CdSe range from 0.02-0.7 using a variety of techniques ranging from resonance Raman to photon echo measurements.[1] Whereas *S* is approximately 10 for bulk CdSe, calculations on strongly confined NCs, where the electron and hole wavefunctions have a greater spatial overlap, predict *S* to be < 0.1.[19] The lack of consistency across the literature played a large part in our motivation to determine the amount of EPC in CdSe NCs. Additionally, we expanded our study to a size-dependent analysis of EPC. EPC strengths have previously been predicted to be size-independent [20], to increase with decreasing size [21] or to have a much more complicated size dependence [22]. Thus, we had clear motivation to determine, through resonance Raman spectroscopy, the extent of EPC in SC NCs and tie those results to any potential size-dependence.

## Experimental Methods

Synthetic methods for semiconductor nanocrystals were originally developed in the late 1980's to early 1990's. Since then, there have been standard procedures published that are highly reproducible. We used procedures that were published by David Kelley's group [23,24] that are based on the pyrolysis of organometallic precursors in a coordinating solvent. These reactions use metal and chalcogen precursors at high temperature in an oxygen free environment to initiate nucleation and subsequent growth of our CdSe nanocrystals, summarized in Appendix I [23]. The type of procedure given in Appendix I gives fairly monodisperse samples with fairly good photoluminescence quantum yield. These techniques were adjusted and refined by the Kelley group to develop separate synthetic procedures for both relatively "smaller," "medium," and "larger" particles as given in Appendix II [24]. These separate synthetic procedures allow one to obtain very monodisperse, highly photoluminescent particles for a large range of sizes. The idea is simply slightly adjusting the Cd to Se ratio, total volume of reaction, type of alkyl phosphine and injection temperature to allow one to adjust the number of initial nuclei forming after injection, *e.g.* the higher the injection temperature, the larger number of initial nuclei form, less starting material is left for growth and therefore smaller particles form.

Nanocrystal sizes were determined using the relationship [25]

$$D = 1.62974 \times 10^{-9}\lambda^4 - 2.85743 \times 10^{-6}\lambda^3 + 1.8873 \times 10^{-3}\lambda^2 - 0.54736\lambda + 59.60816 \quad (4)$$

where D is the diameter in nm and λ is the wavelength of the first absorption maximum in nm. The nanocrystal concentrations were determined using the molar absorptivity determined from the first absorption maximum [25],

$$\varepsilon = \left(\frac{0.06}{\Delta E}\right)\{155{,}507 + 6.67054\, x\, 10^{13} e^{\left(\frac{-E}{0.10551}\right)}\} \quad (5)$$

where ΔE is the half-width at half maximum of the first absorption band in eV (determined by fitting the lower-energy side of the absorption band to a Gaussian) and E is the energy in eV of the first absorption maximum.

Samples used for resonance Raman spectroscopy were dissolved in chloroform at concentrations ranging from 6 to 35 μM. They were contained in 1 mm path length fused silica cuvettes which were placed on the stage of a Jobin-Yvon T64000 Raman microscope system consisting of a 0.64-m triple spectrograph coupled to a confocal Raman microprobe based on an Olympus BX-41 microscope with a 10X objective. The detector was a UV coated, back illuminated, liquid nitrogen cooled CCD with >70% quantum efficiency from 425-800 nm. Spectral resolution was 3-4 $cm^{-1}$ and all spectra were obtained at ambient temperature. Excitation at seven wavelengths from 457.9 to 514.5 nm was provided by a Coherent Innova 90C-5 argon-ion laser. Excitation at 532 nm was obtained from a Spectra-Physics Millennia Vs frequency

doubled, diode-pumped Nd laser, and excitation at 543.5 to 632.8 nm was provided by Melles Griot He-Ne lasers. The laser power measured at the sample did not exceed 1 mW (typically measured powers were about 0.5 mW). For some experiments the sample was translated continuously under the laser in two dimensions using piezo driven stages (Mechonics MS 30 stages with CF 30 controller) to avoid local heating, photocharging, or other undesirable photoinduced changes, but the spectra appeared unchanged in stationary samples at the power levels used. Typically, signal was integrated on the detector for 60 to 120 s before being read out, and 10 to 30 such integrations (15-60 minutes total) were summed to obtain the spectrum of each sample [7].

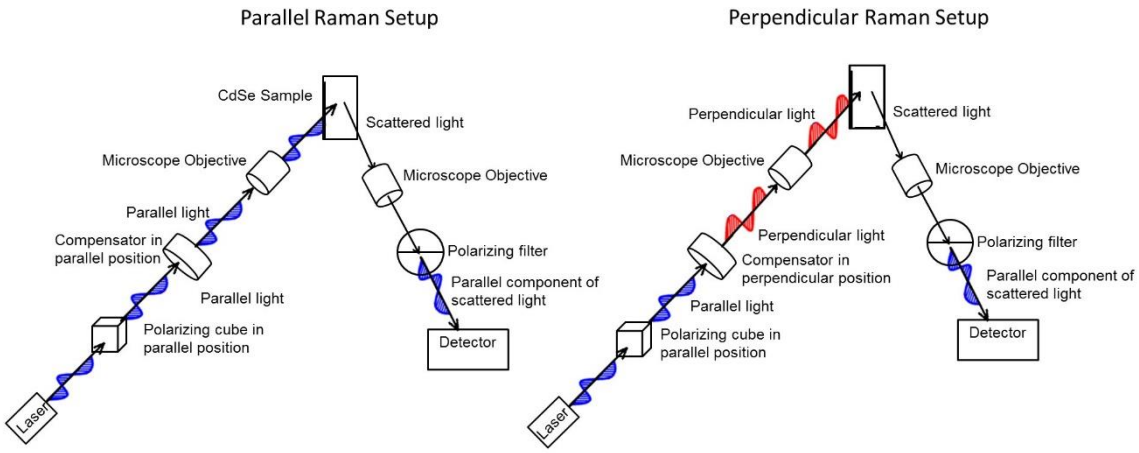


*Figure 6. Left – Resonance Raman experimental setup in parallel position using a compensator to adjust incident laser polarization. Right – Resonance Raman experimental setup in perpendicular position using a compensator to adjust incident laser polarization.*

Our spectrograph contains three gratings, all of which have strongly polarization dependent diffraction efficiencies, so a correction must be used to account for the instrument bias. The correction was obtained by using the depolarization ratio of the 263 $cm^{-1}$ line of chloroform, which has a true depolarization ratio of $\rho_{true} = I_\perp/I_\parallel = 0.75$ as an internal standard. If we say that $E_\parallel$ and $E_\perp$ are the detection efficiencies for initially perpendicular and initially parallel light, respectively, after passage through the imperfect depolarizer, the detected signals for parallel and perpendicular polarizations are $D_\parallel = I_\parallel E_\parallel$ and $D_\perp = I_\perp E_\perp$. The measured depolarization ratio is $\rho_{meas} = D_\perp/D_\parallel = \rho_{true}(E_\perp/E_\parallel)$. This allows us to find the detection efficiency ratio for the two polarizations from the chloroform data as $(E_\perp/E_\parallel) = \rho_{meas}/\rho_{true}$. Then, since the total number of counts is irrelevant, we can define $E_\parallel = 1$ and set $I_\parallel = D_\parallel I_\perp = D_\perp/(E_\perp/E_\parallel)$.

These $I_{\parallel}$ and $I_{\perp}$ spectra were then used to calculate the depolarization ratios for CdSe, and the total differential cross-section spectra were calculated as $I_{\parallel} + I_{\perp}$ [7].

In order to measure the absolute Raman cross sections and depolarization ratios, a polarization analyzer was set to pass the polarization that is most efficiently transmitted through the spectrograph. A Soleil-Babinet compensator was used as a wavelength-tunable half-wave plate to rotate the incoming laser polarization between parallel and perpendicular (Figure 6). In this configuration, the detected signals, $D_{\parallel}$ and $D_{\perp}$, had to be corrected for the differential transmission of the two incoming polarizations through the microscope optics to the sample. This correction was achieved as above by using the measured depolarization ratio of the 263 $cm^{-1}$ chloroform line [7].

Absolute resonance Raman cross-sections were determined from the integrated area of the ~206 LO fundamental peak relative to that of the 667 $cm^{-1}$ chloroform line for which the cross-sections have been previously reported as a function of wavelength [26]. The absolute resonance Raman cross section was calculated using the following relation [7]:

$$\left(\frac{d\sigma}{d\Omega}\right)_{CdSe} = \left(\frac{d\sigma}{d\Omega}\right)_{solv}\left[\frac{(\alpha_L+\alpha_{LO})}{(\alpha_L+\alpha_{solv})}\frac{\left\{1-e^{-2.303(\alpha_L+\alpha_{solv})}\right\}}{\left\{1-e^{-2.303(\alpha_L+\alpha_{LO})}\right\}}\right]\frac{C_{solv}}{C_{CdSe}}\frac{I_{CdSe}}{I_{solv}} \quad (6)$$

Where $\left(\frac{d\sigma}{d\Omega}\right)_{solv}$ is the absolute differential cross-section for the solvent line, $C_{solv}$ and $C_{CdSe}$ are the molar concentrations of the solvent and CdSe, respectively, and $I_{CdSe}$ and $I_{solv}$ are the integrated peak areas from the Raman spectra of the CdSe and solvent, respectively. The quantity in square brackets corrects the observed intensities for the differential reabsorption of the backscattered Raman light. $\alpha_L, \alpha_{LO}$, and $\alpha_{solv}$ are the absorbances of the sample at the laser, scattered LO phonon, and scattered solvent wavelengths, respectively.[7]

Fluorescence spectra and excitation profiles were measured using a Jobin-Yvon Fluorolog-3 spectrometer that consists of a xenon lamp/double-monochromator excitation source and a CCD detector. Quantum yields were determined by comparing the nanocrystal spectra with the spectrum of dilute Rhodamine 6G (R6G) in methanol. The absorbance of the CdSe and R6G samples were small, about 0.1 at 450 nm. The quantum yields are determined by taking the ratio of areas under the luminescence spectra and are corrected for instrument response, monochromator throughput and detector efficiency. The CdSe and R6G spectra are at close to the same wavelengths, therefore the relative correction factors were close to unity. The quantum yield of CdSe is calculated by,

$$QY_{CdSe} = \frac{\left(1-10^{-A_{R6G}}\right)* I_{CdSe}}{\left(1-10^{-A_{CdSe}}\right)* I_{R6G}} * QY_{R6G} \quad (7)$$

where $A_{R6G}$ and $A_{CdSe}$ are the absorbance of R6G and CdSe, respectively. $I_{R6G}$ and $I_{CdSe}$ are the corrected areas under the fluorescence curves of R6G and CdSe, respectively.

$QY_{R6G}$ is the quantum yield of R6G in the dilute methanol solution, with a known quantum efficiency of 95%. In addition to measurement of the quantum efficiency of the NCs, photoluminescence excitation profiles from 440 to 550 nm were measured every 5 nm.

Our synthesized nanocrystals had emission quantum yields typically between 20-30%. This strong emission completely overwhelms the resonance Raman scattering at longer wavelength excitations, where the lowest-energy absorption band is. In order to measure the Raman spectra near the lowest excitonic peak, we had to quench the fluorescence by means of a ligand exchange where the original ligands (octadecylamine and trioctylphosphine) were exchanged with hexadecanethiol, a known hole acceptor [27]. This quenched the fluorescence between one to two orders of magnitude and allowed for us to obtain spectra out to 543.5 nm for the 3.2 nm diameter NCs. The ligand exchange slightly redshifts the absorption spectrum and lowers the intensity of the second excitonic peak relative to the first. To account for any differences that may also occur in the resonance Raman spectra, both the quenched and unquenched nanocrystal spectra for particles approximately 3.2 nm in diameter were taken at excitation wavelengths from 457.9 to 501.7 nm, the range where we could obtain spectra with little fluorescence interference in the unquenched nanocrystals. The comparison between the quenched and unquenched data showed no discernible difference, as I will discuss further in the results section.

Resonance Raman excitation profiles and optical absorption spectra were calculated using the general methods previously described for molecules.[8,9] Each of the electronic states contributing to the optical absorption or Raman enhancement was assumed to be polarized either along the z axis (the unique axis in the wurtzite crystal structure) or degenerate in the xy plane. We assumed the Condon approximation where the transition dipole moment to an excited vibronic state separates into the product of a purely electronic transition dipole and a purely vibrational overlap integral. We use linearly polarized excitation and detect scattered light propagating in a direction perpendicular to that of the incident polarization, polarized either parallel or perpendicular to the incident polarization. The differential Raman cross sections for parallel and perpendicular detection for a transition between ground-state phonon levels i and f is given by[48,49] (in SI units)[50]

$$\left(\frac{d\sigma_{if}}{d\Omega}\right)_{\parallel} = \frac{\omega_L \omega_S^3}{16\pi^2 \varepsilon_0^2 \hbar^2 c^4} \frac{1}{15} \left[8\left|\alpha_{xx,if}\right|^2 + 3\left|\alpha_{zz,if}\right|^2 + 4Re\left(\alpha_{xx,if}^* \alpha_{zz,if}\right)\right] \tag{8a}$$

$$\left(\frac{d\sigma_{if}}{d\Omega}\right)_{\perp} = \frac{\omega_L \omega_S^3}{16\pi^2 \varepsilon_0^2 \hbar^2 c^4} \frac{1}{15} \left[\left|\alpha_{xx,if}\right|^2 + \left|\alpha_{zz,if}\right|^2 - 2Re\left(\alpha_{xx,if}^* \alpha_{zz,if}\right)\right] \tag{8b}$$

where $\omega_L$ and $\omega_S$ are the laser and scattered frequencies. The components of the Raman polarizability tensor are calculated in the time domain as

$$\alpha_{kk,if} = \sum_e M_{e,k}^2 \int_0^\infty dt < f|i(t) >_e \exp[i\left(\omega_L - \omega_{eg} + \omega_i\right)t - g_e(t)] \tag{9}$$

where e is an electronic (electron-hole) state, $M_{e,k}$ is the electronic transition dipole moment between the ground state and excited state e along direction k (in a nanocrystal-fixed coordinate system), $\omega_{eg}$ is the frequency difference between the purely electronic states, and $g_e(t)$ is a damping function that accounts for all sources of electronic homogeneous dephasing. As discussed further below, we model the homogeneous dephasing as coupling to an overdamped Brownian oscillator [45,51] with the explicit expression for $g_e(t)$ given in Eqs. (8.48) of Ref. 51. The quantity $|i(t)>_e = e^{-iH_e t/\hbar}|i>$ is the initial ground-state phonon wavefunction propagated on the potential energy surface for excited state e. Equations (8) do not explicitly include inhomogeneous broadening which can arise from a distribution of sizes or shapes within the ensemble of sampled nanocrystals. These effects were handled by averaging Eqs. (8) over a Gaussian distribution of energy gaps $\omega_{eg}$. Note that while the homogeneous dephasing enters the Raman equations at the level of the quantum mechanical amplitude (the Raman polarizability), the inhomogeneous broadening appears as an average over cross-sections, the polarizability squared. In addition, if multiple i→f phonon transitions have experimentally indistinguishable frequencies, each cross-section must be calculated separately and then summed for comparison to experiment. Although atomistic simulations[19] suggest that the LO phonon in nanocrystals actually has contributions from several nearly degenerate phonon modes that involve the same motion at the unit cell level but different phases and amplitudes across the crystal, a single phonon mode was assumed in the calculations for simplicity. In addition, at ambient temperatures the phonon modes have considerable Boltzmann population in states other than v = 0. The calculations included a Boltzmann-weighted sum over the v = 0, 1, and 2 initial states, which account for about 95% of the initial population at 298 K. In the present case where the cross-sections are averaged over an inhomogeneous distribution, the resonance Raman depolarization ratio corresponding to what we measure is calculated directly from Eqs. (8) as

$$\rho = (d\sigma_{if}/d\Omega)_{\perp}/(d\sigma_{if}/d\Omega)_{\parallel} \tag{10}$$

Finally, the corresponding electronic absorption spectrum is given in SI units by[48,50]

$$\alpha_A(\omega) = \frac{\omega}{3n\varepsilon_0\hbar c}\sum_e G_e M_e^2\, Re \int_0^\infty dt < i|i(t)>_e \exp[i(\omega - \omega_{eg} + \omega_i)t - g_e(t)] \tag{11}$$

where n is the solvent refractive index and *Re* designates the real part of the complex quantity. $G_e$ is the degeneracy of excited state e: $G_e = 1$ for z-polarized transitions and $G_e = 2$ for xy polarized transitions. Again, inhomogeneous broadening is handled by averaging this expression over a Gaussian distribution of $\omega_{eg}$, and a Boltzmann-weighted sum over initial levels i is performed.

The fluorescence bandshape is calculated as[53]

$$I_F(\omega)\ \alpha\ \omega^3 \sum_e G_e\, M_e^2\, Re \int_0^\infty dt < v|v(t)>_e \exp[i(-\omega + \omega_{eg} + \omega_v)t - g_e(t)] \tag{12}$$

where v is a phonon level of excited state e and $|v(t)>_e = e^{-iH_g t/\hbar}|v>$ is this phonon state propagated for time t on the ground-state potential energy surface. The thermal distribution of initial states includes the phonon levels of the two lowest electronic states in our calculations.

As the resonance Raman and electronic spectra depend on all of the same spectroscopic parameters, we require that our modeling parameters simultaneously reproduce the measured absorption spectrum, the emission band shape, the total resonance Raman excitation profile $(\frac{d\sigma_{if}}{d\Omega})_{\parallel+\perp}$ (the sum of Eqs. (8a) and (8b)) in absolute units for the LO phonon fundamental, the depolarization ratio for the LO fundamental, and the LO overtone to fundamental ratio.

## Computational Considerations

Resonance Raman spectra contain much information about the photophysics that accompany optical excitation of a material. In the simple limit of a single resonant electronic excitation and linear electron-phonon coupling, the resonance Raman excitation profile depends on the electron-phonon coupling strength, the oscillator strength of the electronic transition, and the electronic spectral broadening (inhomogeneous broadening and homogeneous electronic dephasing). Additionally, the optical absorption spectrum depends on the oscillator strength of the electronic transition and electronic spectral broadening. Consequently there are a set of parameters that provides adequate best fits to the absorption spectrum and the Raman profiles.

An absorption spectrum is simply the sum of the contributions from each contributing state while the resonance Raman spectrum may have intermediate resonances that add complex-valued amplitudes that are then squared to give the Raman observables. Partially overlapping electronic excitations in Raman profiles may create interferences that cause the Raman profiles to be more structured than the absorption and in turn, eliminate any simple relationship between the two, making the modeling parameters more difficult to determine.

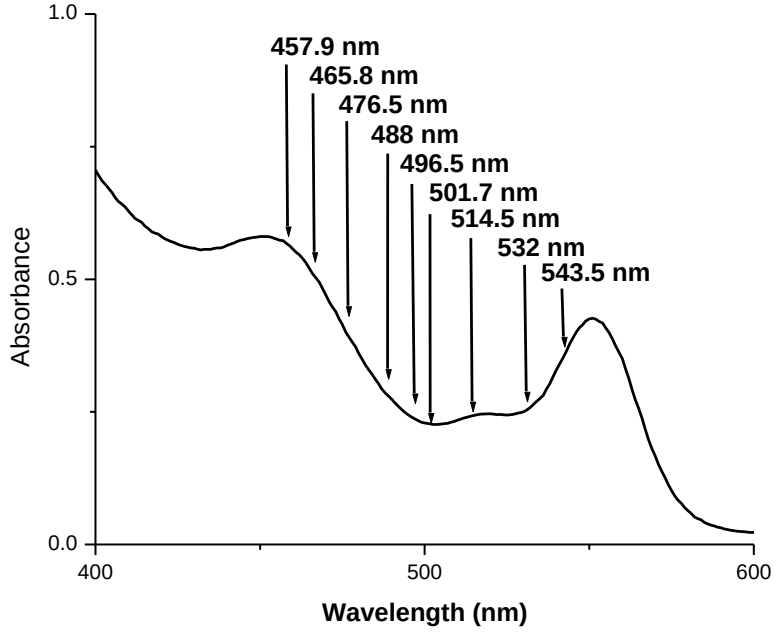


*Figure 7. Excitation wavelengths used with respect to CdSe linear absorption spectrum of NCs 3.2 nm in diameter.*

The excitation wavelengths used in this study span the three lowest-energy resolved features in the optical absorption spectrum (Figure 7). These transitions are usually assigned using the effective mass approximation envelope function model as shown in Figure 2. The first band, at ~557 nm in our sample, is assigned as $1S_{3/2}$-$1S_e$, the second, weaker band, at ~526 nm in our sample, is assigned as $2S_{3/2}$-$1S_e$, while the strong, broad band at ~458 nm is often labeled as $1P_{3/2}$-$1P_e$ but has significant contributions from other transitions.[28-32] The calculations of Wang and Zunger on smaller CdSe NCs[33] place at least eight different transitions with significant oscillator strength in the first ~0.5 eV above the lowest excitonic transition, which is roughly the region spanned by the first three observable peaks in the experimental absorption spectra. Reference 7 covers much of the background information used to parameterize our computer modeling as well as initial fitting of CdSe NCs.

In the interest of simplicity, we started by following work similar to that of the Alivisatos,[17] where we used a 3-transition model centered about each of the resolved features in the absorption spectrum (Figures 13 and 14). As discussed in more detail in Reference 7 and below, modeling with this assumption reproduced the experimental absorption and resonance Raman cross sections well while the depolarization ratios and overtone to fundamental ratios were greatly deviant.

Further consideration of the fine structure of each excitonic transition of the CdSe wurtzite lattice introduces crystal field splitting and the electron-hole exchange interaction. This splits each of the lowest-energy transitions into five different energy levels, two of which are z-polarized and three doubly degenerate xy-polarized transitions, as shown in Figure 3.[28] The distribution of the oscillator strength between the ±1L and ±1U transitions and the energetic splittings among all states, depend on the size and precise shape of the NCs.[29] In general, the lower-energy transitions consist of xy-polarized and z-polarized components having similar oscillator strengths and small energetic splittings (xy being lower in energy), while the pattern becomes less regular at higher energies.[29-30]

With consideration of the fine structure, we adjusted our modeling parameters to include xy- and z-polarizations for each of the lower-energy transitions which allowed us to fit the somewhat lower than 1/3 ($\rho = 1/3$ for a linear oscillator) depolarization ratios in our 3.2 nm diameter NCs. In our original studies, we found that an 8-transition model worked well to fit our data, where the first three transitions were split into their xy- and z-polarized components and the two highest energy transitions were only z-polarized.[7] After that study, we adjusted our synthetic method slightly to give higher quality, more monodispersed NCs. With these NCs, we found that the depolarization ratios and overtone to fundamental ratios were somewhat lower at higher energies and therefore, the xy- and z-polarized components needed to be included in the higher energy spectral region. For these higher quality particles mentioned below, we found that optimizing our fits to a 9-transition model (where the first four lowest energy transitions were split into xy- and z-components while one higher energy transition was solely z-polarized) was needed to fit the depolarization

ratios and overtone to fundamental ratios at higher energies. All of these results are discussed in more detail below in the results section.

Inhomogeneities in nanocrystal size, shape and surface chemistry are all factors that have a significant contribution to the linewidth of the electronic spectra. Even in the most monodisperse nanocrystal samples, inhomogeneities in crystal size, shape, and surface chemistry exist. High quality samples of CdSe NCs typically have a half-width at half maximum, measured on the low-energy side of the first absorption maximum, of 400–500 $cm^{-1}$. This width is typically assumed to be primarily inhomogeneous while a small amount is from homogeneous broadening. In addition, there is a contribution to the width from the excitonic fine structure discussed above. All of the observed features in the optical spectrum shift with particle size in the same direction and at about the same rate, so we assumed that the inhomogeneous broadening of each transition is fully correlated. Therefore, we calculated the absorption and emission spectra and the Raman profiles for a single nanocrystal followed by convolution with a Gaussian distribution to obtain the ensemble-averaged spectra.

One must also include the different effects quantum confinement has on sizes of NCs. As mentioned in the introduction, the energy gap of NCs increases as the radius decreases. When one considers the fine structure, this change in size and energy gap also changes the splitting between transitions.[29] As one decreases the size of the NC, the energy spacing between transitions also becomes larger. Additionally the amount of inhomogeneity can affect the fitting parameters. As one decreases the size of NCs, the amount of inhomogeneity is expected to increase due to the nature of our high temperature synthesis. In large part, the reactions for smaller NCs occur at a higher injection temperatures and shorter times which leads to an increased probability that there with be inhomogeneities in NC size, shape, and surface chemistry. Similarly, with homogeneous broadening, it is expected to increase as the NC size decreases.

As mentioned above, part of the reasoning for undertaking this project was due to the controversy in the literature for the amount of electron-phonon coupling present in CdSe NCs. Many arguments are put forward to determine what trends should occur based on NC size.[20-22] It has been understood that reducing the size of the NC leads to a greater overlap between the electron and hole wavefunctions due to quantum confinement. Calculations have shown that strongly confined NCs have a very small Huang-Rhys parameter ($S < 0.1$)[22]. While in Reference 22 it is claimed that EPC has a complicated size dependence, we may expect all strongly confined NCs EPC to be similar and independent of size, consistent with Reference 20, because it is unclear as to what size the NC has to be in order to not feel the strong confinement effect.

## Results

Absorption spectra for both quenched and unquenched CdSe nanocrystals are shown in Figure 8. These as-synthesized particles showed a first excitonic peak at 551 nm (3.2 nm diameter particles) and a weakly resolved second excitonic peak at 519 nm. The quenched particles showed a red-shift of the lowest-energy transition of 6 nm to 557 nm while maintaining the same band shape with no apparent broadening. The second transition however loses intensity to where it is no longer clearly resolved. We believe this is caused by the hexadecanethiol ligands lowering the energy of the hole at the edge of the crystal, allowing the $1S_{3/2}$ wavefunction to expand slightly. This lowers the energy and causes the red-shift in the absorption spectrum. We believe this causes the $1S_{3/2}$ hole wavefunction to have greater overlap with the $1S_e$ electron wavefunction while decreasing its overlap with the $2S_e$, causing the changes in the first two excitonic transitions.

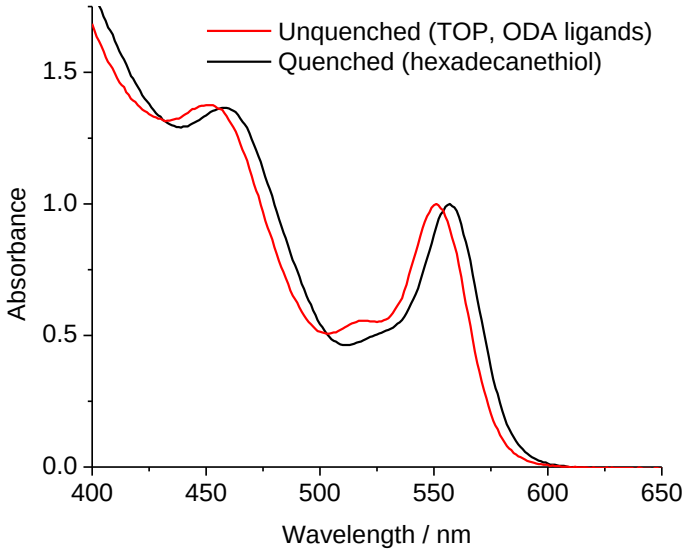


*Figure 8. Linear absorption spectra for quenched and unquenched nanocrystals approximately 3.2 nm in diameter.[7]*

To verify the red-shift in the absorption spectrum had little to no effect on the coupling to the LO phonon, we ran both quenched and unquenched NCs using excitations from 457.9 to 501.7 nm (Figure 9), the range where we could obtain spectra for both NCs. These spectra showed no discernible difference between the measured Raman cross sections or the resonance Raman spectra.

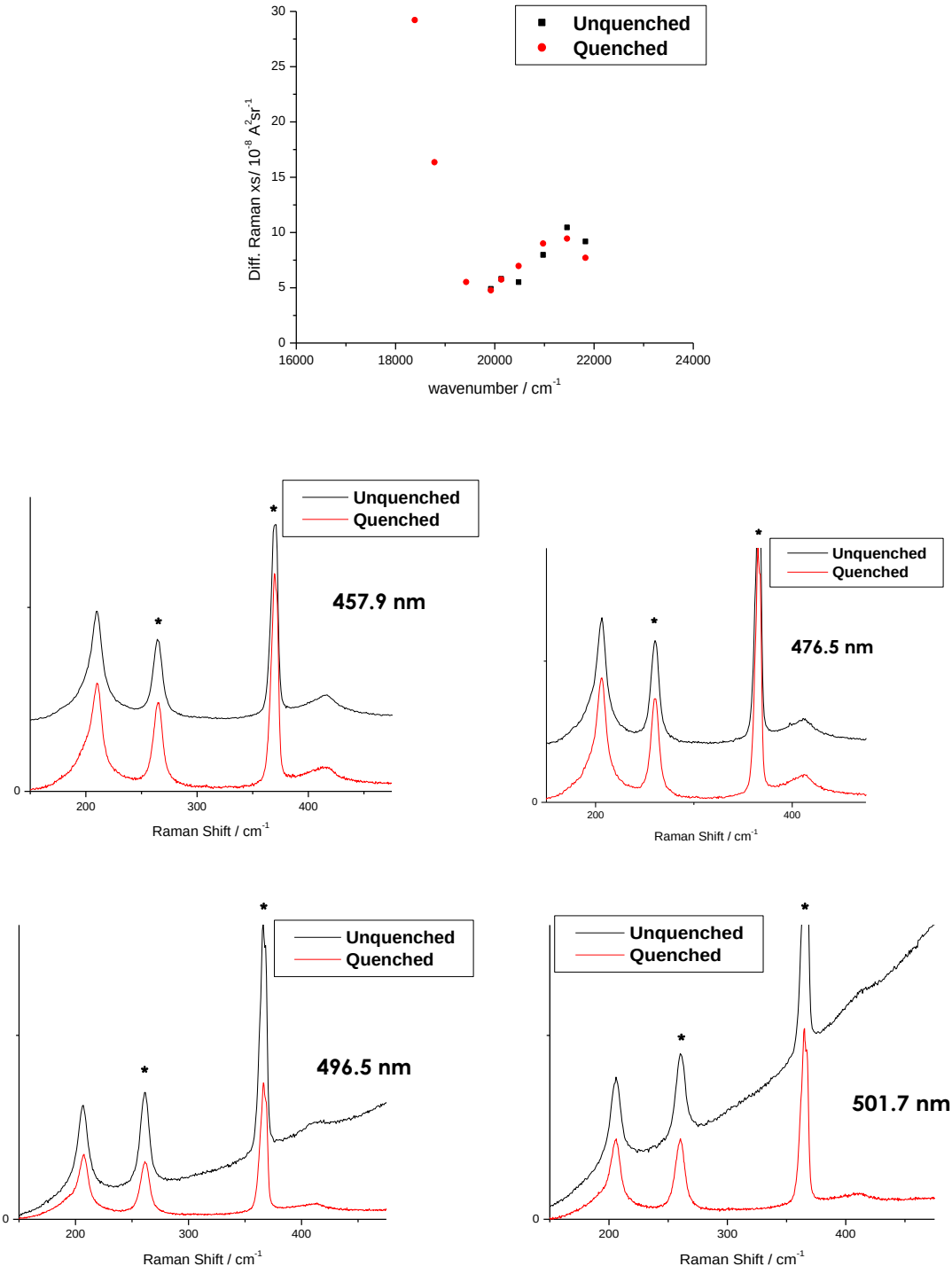


*Figure 9. Top, comparison of resonance Raman cross sections for quenched versus unquenched particles (3.2 nm in diameter). Bottom, resonance Raman spectra at indicated excitation wavelengths for quenched versus unquenched samples, with chloroform solvent peaks labeled with an asterisk (*) [7].*

Figure 10 shows representative polarized and depolarized resonance Raman spectra of CdSe NCs in chloroform at three excitation wavelengths. The dominant CdSe feature in all of our spectra is the LO phonon centered about 206-208 $cm^{-1}$. In all cases, the LO phonon has an unresolved shoulder on the low frequency side of the band. We also observed the overtone of the LO phonon at approximately 412 $cm^{-1}$ which is just about two times the frequency of the LO fundamental, coinciding with it being the two-quantum transition. The overtone is very broad and it is difficult to determine its integrated intensity accurately. In some of the higher-energy transitions, the three-quantum transition can be seen at about 615 $cm^{-1}$, however no effort was made to quantitate its intensity.

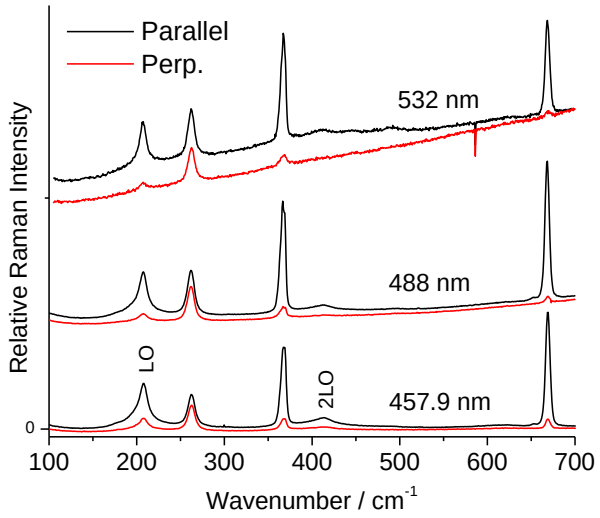


*Figure 10. Representative resonance Raman spectra of CdSe NC's (3.2 nm in diameter) in chloroform at the indicated excitation wavelengths. The LO phonon fundamental and overtone are labeled; Concentrations for are 22.9 μM for the 457.9 and 488 nm spectra and 8.86 μM for the 532 nm spectrum. [7]*

Comparison of the parallel and perpendicular spectra in Figure 10 shows that the LO phonon has a degree of polarization between that of the 263 $cm^{-1}$ and 667 $cm^{-1}$ chloroform Raman lines which are strongly depolarized and polarized, respectively. As mentioned before, there was negligible underlying fluorescence in the shorter excitations of the unquenched samples but the fluorescence rises until it nearly swamps the Raman scattering at an excitation of 514.5 nm. In the quenched samples however, we were able to obtain spectra out to excitations of 532 and 543.5 nm for 3.2 nm diameter nanocrystals, although there is still a considerable background that compromises the signal to noise of the Raman features.

In our original studies using particles approximately 3.2 nm in diameter, evaluation of the resonance Raman cross sections for the LO fundamental using Eqn. (6) yields cross sections that drop from about 2 x $10^{-7}$ $Å^2$ $sr^{-1}$ at the 543.5 nm excitation to about

5 x $10^{-8}$ Å$^2$ sr$^{-1}$ at the 501.7 nm excitation and then rise gradually between 8-10 x $10^{-8}$ Å$^2$ sr$^{-1}$ between the 476.5 – 457.9 nm excitations. The depolarization ratios were slightly lower than 1/3 at the shortest excitation wavelengths and become smaller at longer wavelengths. At the longer wavelength excitations where the fluorescence background rises greatly it was difficult to measure the peak intensity accurately, however it is obvious from the spectra that the depolarization is significantly smaller than 1/3 (Figure 10). Overtone to fundamental ratios were between 0.5-0.6 at the shortest excitation wavelengths and fall steadily as the excitation is moved to longer wavelengths. Again the overtone, like the depolarization, is difficult to measure when the fluorescent background is strong at the longer excitation wavelengths, however from Figure 10, one can see that the relative intensity decreases as one tunes to longer excitation wavelengths. In comparison, Shiang *et al.* previously reported that the overtone to fundamental ratio "seems roughly constant" with excitation wavelength, [16] however no data was shown to support this and their samples may have been less monodisperse than ours. Our previous studies [18] have shown that in polydisperse samples the excitation wavelength dependence is greatly reduced when compared to monodisperse samples.

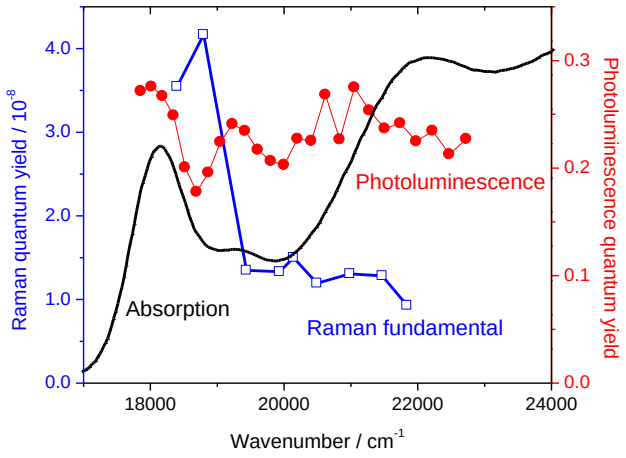


*Figure 11. Comparison of the absorption spectrum (black curve, arbitrarily scaled), the LO Raman fundamental quantum yield (blue, left-hand axis), and photoluminescence quantum yield (red, right-hand axis). [7]*

Figure 11 shows a comparison of the absorption spectrum, photoluminescence quantum yield, and the Raman quantum yield. The Raman quantum yield is obtained by multiplying the differential Raman cross section by $(\frac{8\pi}{3}\frac{1+2\rho}{1+\rho})$ to convert to total cross section,[9] and then dividing by the absorption cross section. The photoluminescence yield was fairly consistent across the entire absorption band, however it did show a bit more structure then the corresponding absorption spectrum, with more resolved peaks at the position of the first two excitonic peaks. The Raman quantum yield was about six orders of magnitude smaller and seems to be much more

excitation wavelength dependent with nearly constant values across the 457.9 to 514.5 nm range but then rises greatly near the first exciton.

Studies conducted nearly 20 years ago by the Alivisatos group modeled their data using only three electronic transitions centered about the weakly resolved features in their absorption spectrum.[17] Following Alivisatos, we initially attempted to model our experimental data using three electronic transitions centered at about 557, 526, and 458 nm as observed in Figure 8. Additionally, we assumed that the first and third transitions were z-polarized and the weaker, second transition is xy-polarized.[17]

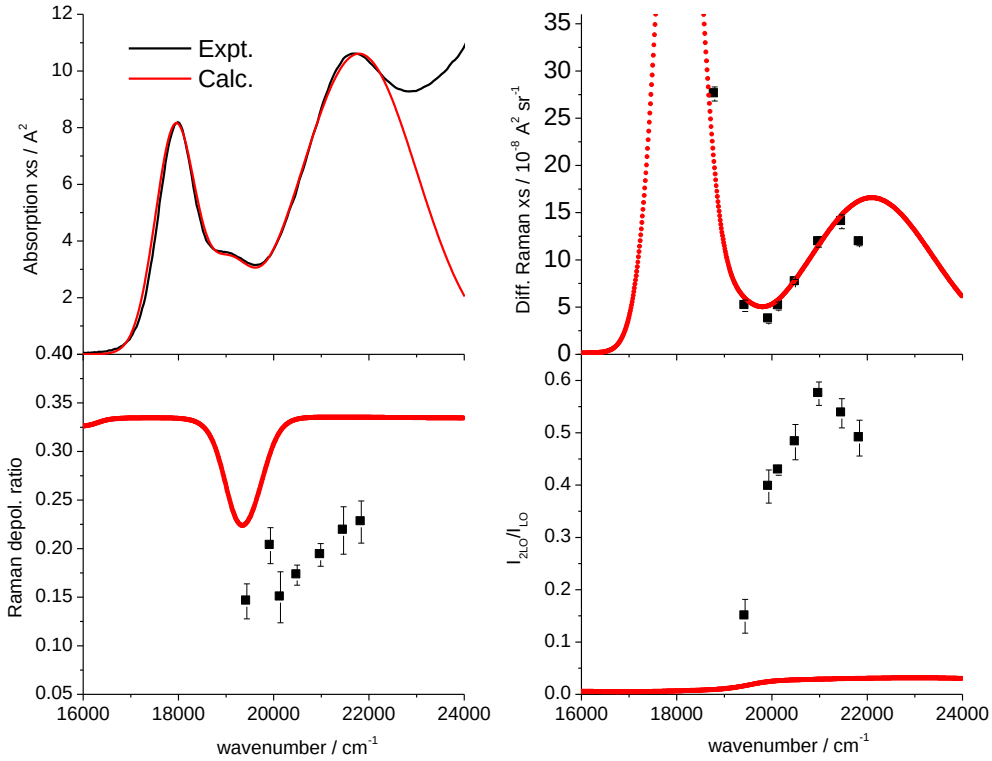


*Figure 12. Experimental and calculated absorption spectrum, fundamental Raman excitation profile, fundamental Raman depolarization ratio, and overtone to fundamental ratio for a model assuming an inhomogeneous width of 1000 cm$^{-1}$ (FWHM) and three electronic transitions having center frequencies of 17930, 19025, and 21750 cm$^{-1}$, homogeneous widths of 50, 50, and 2600 cm$^{-1}$, transition lengths of 2.72, 1.03, and 4.81 Å, and Huang-Rhys factors of 0.0032, 0.0032, and 0.78, respectively.*

Fitting the experimental absorption spectrum to just three transitions requires that the highest-energy transition have a high oscillator strength, at least three times that of the lowest-energy transition, and a very large width. Even with assuming fully

correlated inhomogeneous broadening and just enough homogeneous broadening to fit the first excitonic peak to fit, the highest-energy transition must have a very large homogeneous width, at least an order of magnitude greater. Figure 12 shows the calculated fits to the absorption spectrum, LO phonon fundamental Raman excitation profile, LO fundamental depolarization ratio, and LO phonon overtone to fundamental intensity ratio under the assumption that the lowest transition is almost entirely inhomogeneously broadened.

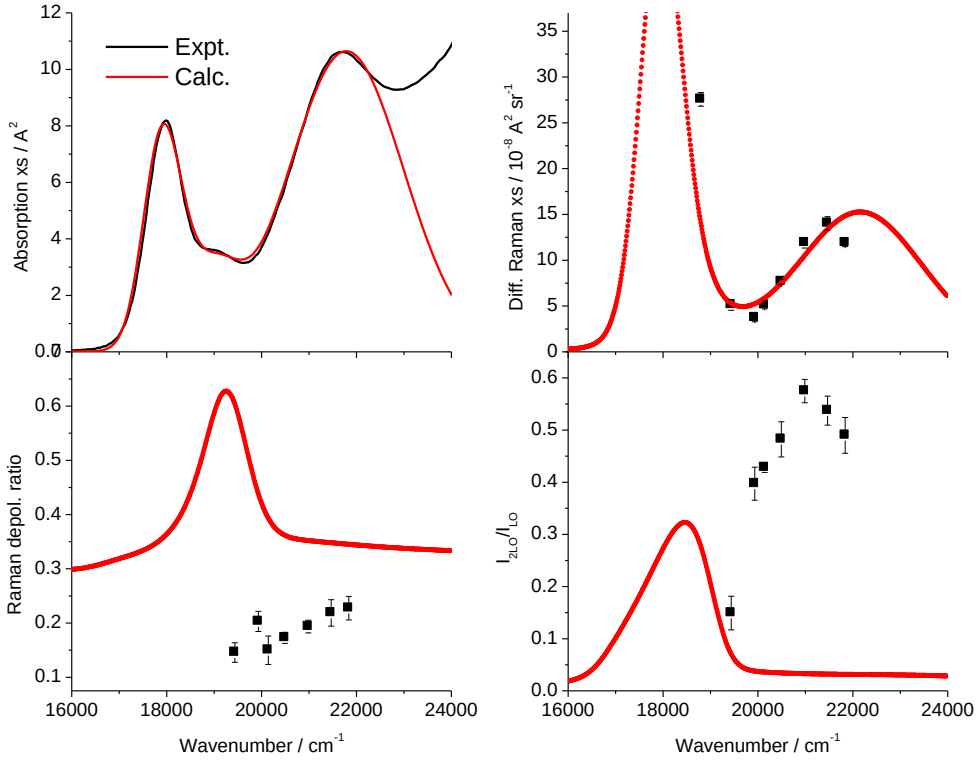


*Figure 13. Same as Figure 12, but assuming zero inhomogeneous broadening. The three electronic transitions have center frequencies of 17935, 19010, and 21750 cm$^{-1}$, homogeneous widths of 750, 1100, and 2750 cm$^{-1}$, transition lengths of 2.64, 1.12, and 4.81 Å, and Huang-Rhys factors of 0.91, 0.405, and 0.91, respectively.*

Figure 13 shows the same calculations, however in the limit of zero inhomogeneous broadening, opposite that of Figure 12. In both cases the absorption spectrum and Raman excitation profile are fit quite well, but the calculated overtone intensities at higher excitation energies are far too low as well as the LO fundamental depolarization ratios far too high at lower energies. The overlap integral requires more time to develop for an overtone than for a fundamental, therefore the large linewidth of the highest-energy state reduces the overtone intensity to nearly zero. The overtone intensity can be increased by increasing the Huang-Rhys factor in the model, but consequently the fundamental Raman intensity is too high. As for the

experimental depolarization ratios, the mostly inhomogeneous broadening model (Figure 12) gave depolarization ratios that are about one-third except when it is directly on resonance with the xy-polarized transition. The purely homogeneous broadening model (Figure 13) predicts depolarization ratios that are too high, especially in regions where the z-polarized and xy-polarized transitions overlap strongly. This approaches the behavior expected for a spherically symmetric system. Calculations using intermediate combinations of homogeneous and inhomogeneous broadening produce intermediate results, however both the overtone intensities and the depolarization ratios still deviate considerably from experiment.

The Huang-Rhys factor required to fit the Raman LO fundamental intensity depends strongly on the homogeneous linewidth. S for the lowest-energy transition varies by a factor of nearly 500 over the range of extremes presented in Figs. 12 and 13. When the balance between homogeneous and inhomogeneous broadening is constrained to correctly reproduce the experimental Stokes shift of the emission (Figure 14), the best fit value of S for the lowest transition is found to be about 0.18 with this simple three transition model.

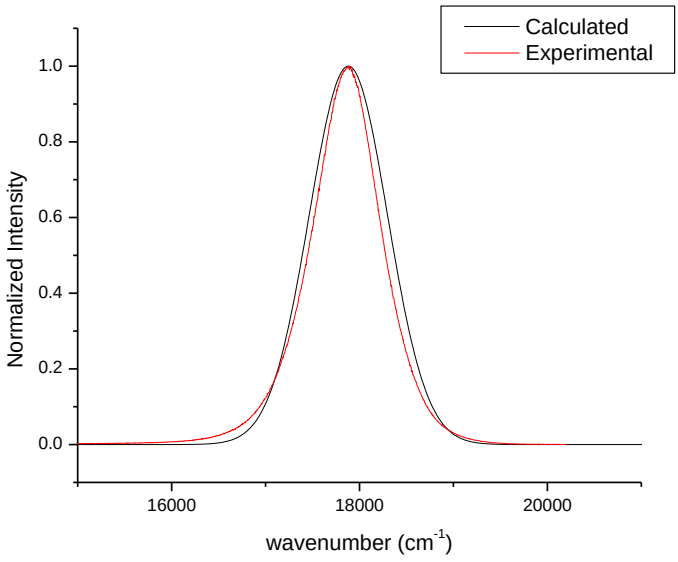


*Figure 14. Experimental and calculated emission spectra for 3.2 nm diameter CdSe nanocrystals.*

The deviation between this model and the experimental depolarization ratios can be accounted for by the lack of a mixture of xy- and z-polarized components. As mentioned above, the fine structure has both xy- and z-polarized components in the first excitonic band. Additionally, the fact that the overtone intensities cannot be reproduced at higher excitation energies is a result of this broad band containing multiple excitonic transitions, not one with a very large linewidth. Following Norris and Bawendi's low temperature photoluminescence excitation fits[32], we tried to constrain our model to the five lowest-energy transitions. The four lowest energy

excitations were modeled using xy- and z-polarized pairs having the same linewidth and Huang-Rhys factor for each transition. Each xy-polarized transition had twice the total oscillator strength of the z-polarized transition and was 150 $cm^{-1}$ lower in energy, the approximate separation between the $0^U$ and the center of the $\pm1^L$ and $\pm1^U$ transitions for spherical wurtzite crystals of 3.2 nm diameter.[29] For CdSe NCs with a first excitonic transition at 557 nm (2.23 eV), the next four excitonic transitions were taken to lie at 1090, 2050, 3380, and 4130 $cm^{-1}$ higher in energy.[32] These initial values had to be adjusted slightly to better fit our data. The higher-energy transition was assumed to be purely z-polarized based on the nearly 1/3 Raman depolarization ratios at the shorter excitation wavelengths.

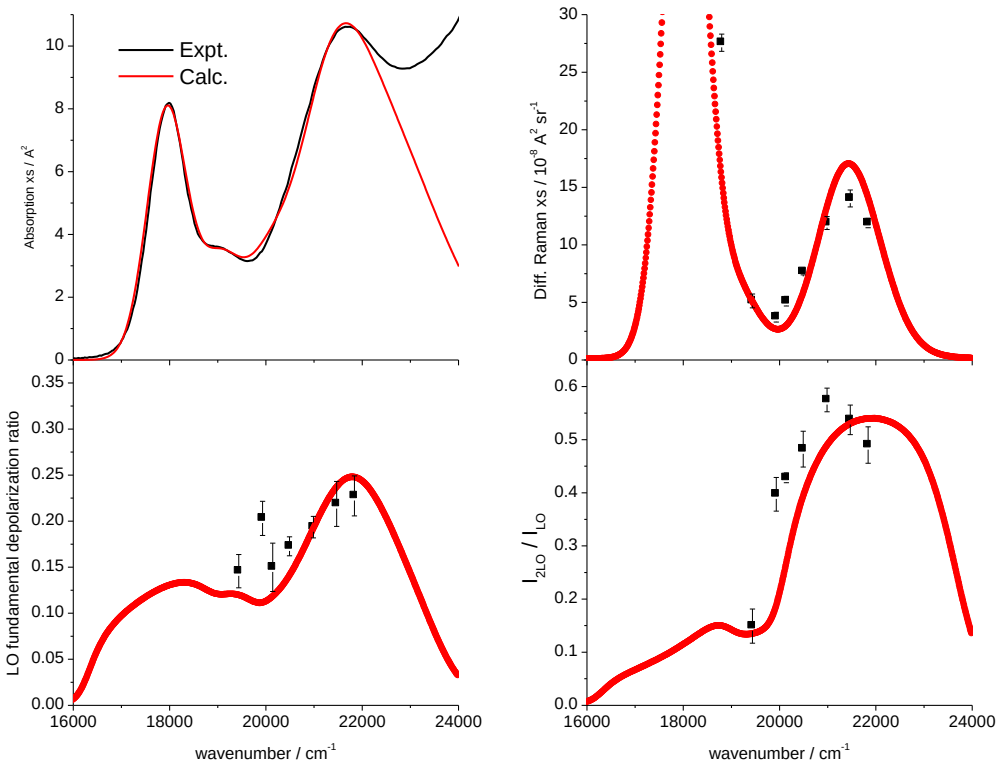


*Figure 15. Same as Fig. 13 but for a 9-transition model (four xy/z pairs and one higher energy state). Parameters of the model are given in Table 1.*

After exploring a large number of parameter sets based on these starting points, it was concluded that much of the absorbance in the broad band near 458 nm must come from multiple transitions, one or more transitions that have large oscillator strengths but contribute negligibly to the Raman intensity and one or more transitions that contribute strongly to the Raman intensity and negligibly to the oscillator strength. This appears to be the only way to rationalize the relatively low absolute Raman cross-sections for the LO fundamental together with large overtone to fundamental intensity ratios in the 20000-22000 $cm^{-1}$ region. Figure 15 compares the calculated

and experimental results from the best-fit parameters given in Table 1. Also shown in that table are the assignments of these transitions by Norris and Bawendi.[32]

*Table 1. Final modeling parameters for CdSe NCs approximately 3.2 nm in diameter. Inhomogeneous width = 890 cm$^{-1}$, refractive index = 1.49 [7]*

| center frequency / cm$^{-1}$ | homogeneous width (FWHM) / cm$^{-1}$ | transition length / Å | polarization | S | assignment (ref. 32) |
|---|---|---|---|---|---|
| 17890 | 250 | 1.55 | xy | 0.08 | $1S_{3/2}1S_e$ |
| 18040 | 250 | 1.55 | z | 0.08 | |
| 18980 | 270 | 0.86 | xy | 0.08 | $2S_{3/2}1S_e$ |
| 19130 | 270 | 0.86 | z | 0.08 | |
| 19940 | 300 | 0.56 | xy | 0.08 | $1S_{1/2}1S_e$ (?) |
| 20090 | 300 | 0.56 | z | 0.08 | |
| 21275 | 400 | 1.05 | xy | 1.53 | $1P_{3/2}1P_e$ |
| 21775 | 400 | 1.05 | z | 1.53 | |
| 22025 | 3000 | 4.45 | z | 0 | |

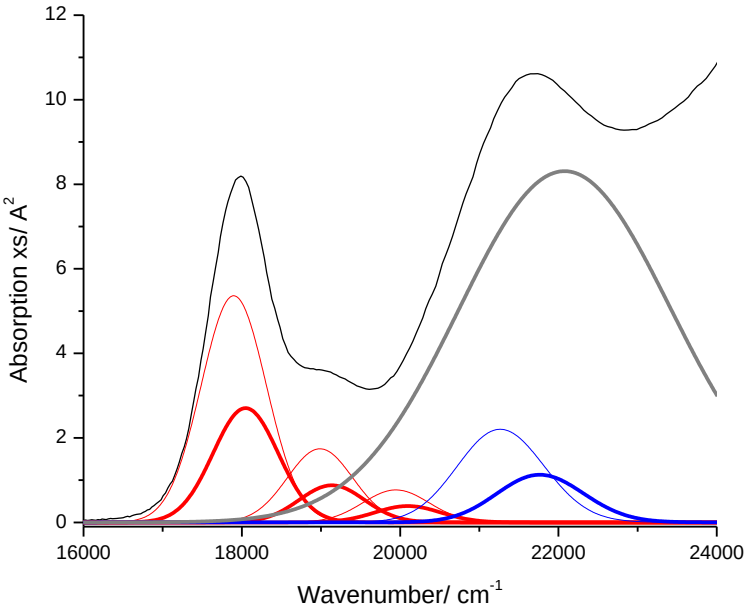


*Figure 16. Experimental absorption spectrum and the nine components of the calculated absorption spectrum (3.2 nm diameter nanocrystals) as given by the fitting parameters of Table 1. Thick and thin lines indicate z-polarized and xy-polarized transitions, respectively. Grey, red, and blue curves represent states having zero, small, and large Huang-Rhys factors, respectively. The xy-polarized transitions are twice as intense as the corresponding z-polarized transitions because of their degeneracy.[7]*

Figure 16 displays the resulting composition of the absorption spectrum. The very broad band at 22150 $cm^{-1}$ surely contains multiple transitions, but a great amount of the absorbance in the 20000-22000 $cm^{-1}$ region must come from transitions that make little contribution to the LO fundamental Raman scattering. The six lowest-energy transitions (red curves in Fig. 16) are assumed to have identical Huang-Rhys factors between each xy- and z-polarized transitions, but these parameters, particularly for the weaker bands, can be varied considerably without greatly affecting the quality of the fits.

We continued with a size dependent study of our CdSe NCs. As mentioned before, there has been some discussion as to the trend one expects when analyzing different sized NCs. [1, 20-22] With this in mind, we synthesized various sized particles by adapting small variations from previously reported literature, similar to what is reported in Appendix I. [24] These syntheses enabled us to yield different sized particles that absorbed at about 522, 538, 551, and 613 nm. Following our initial studies, we performed a ligand exchange with hexadecanethiol on each sample prior to performing Raman measurements to quench the underlying fluorescence. The resulting wavelengths from each ligand exchange are summarized in Table 2. All of the smaller NCs (<3.5 nm diameter) showed an absorption shift of between 6-8 nm whereas our largest NCs (5.2 nm diameter) showed no absorption shift of the first exciton. The lack of shift in the absorption spectrum for the 5.2 nm diameter particles could be attributed to the fact larger NCs energy spacing between transitions was smaller.[54] Additionally, this size-dependent shift in the absorption spectra could be attributed to changes in the strength of confinement within the NCs.[62] While the first exciton absorption didn't shift in energy for the 5.2 nm NCs, the second transition did lose intensity to where it was no longer clearly resolved as was seen in all of our other NCs.

*Table 2. Absorption wavelength of first excitonic transition before and after quenching for various sized CdSe NCs.*

| Nanocrystal Size (nm) | Wavelength Before Quenching (nm) | Wavelength After Quenching (nm) |
|---|---|---|
| 2.8 | 522 | 528 |
| 3.0 | 538 | 545 |
| 3.2 | 551 | 557 |
| 5.2 | 613 | 613 |

*Table 3. Final size dependent Huang-Rhys factors of the lowest energy exciton ($S_{LEX}$) and the higher energy spectral region ($S_{HE}$) using a 9-transition model.*

| Particle Diameter | $S_{LEX}$ | $S_{HE}$ | |
|---|---|---|---|
| 2.8 nm | 0.08 | 0.72 | 0 |
| 3.0 nm | 0.08 | 0.78 | 0 |
| 3.2 nm | 0.08 | 1.53 | 0 |
| 5.2 nm | 0.08 | 1.53 | 0 |

Initial attempts to study size-dependent EPC suffered from poor sample homogeneity which made the data unreliable. Inhomogeneities in nanocrystals lead to different sized NCs within the ensemble that may be on resonance with higher energy excitations and therefore, would cause a much larger Raman cross section at higher energies. Therefore, final analyses were carried out using only "good" samples as defined by the paragraph below.

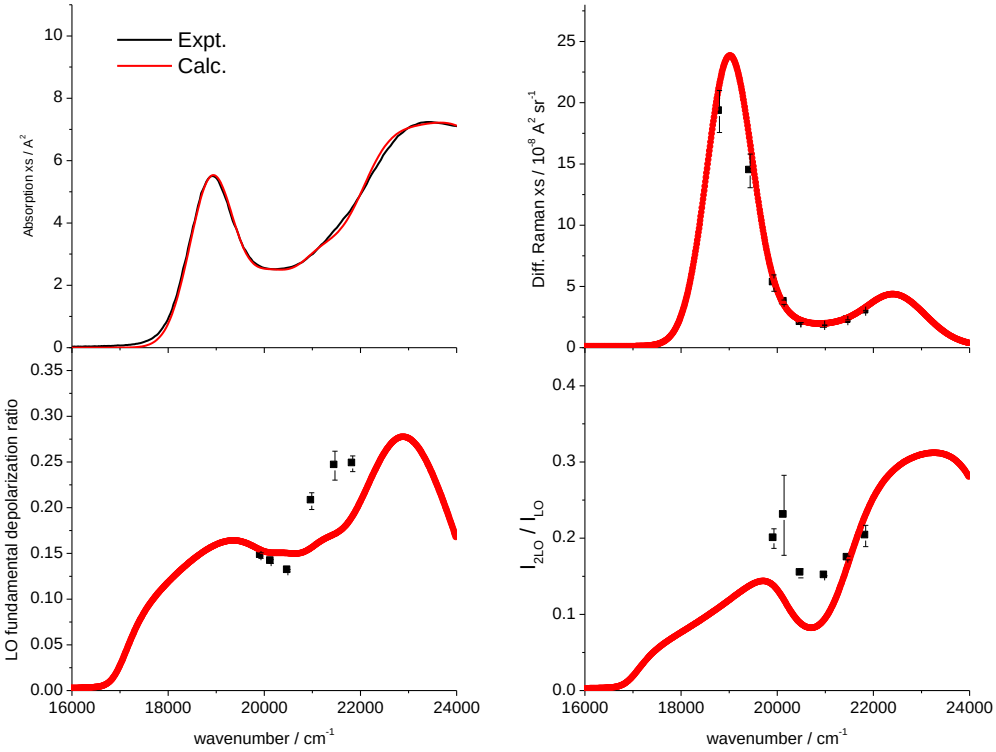


*Figure 17. Experimental and calculated absorption spectrum, fundamental Raman excitation profile, fundamental Raman depolarization ratio, and overtone to fundamental ratio for nanocrystals 2.8 nm in diameter. This model assumes 9-transitions (four transitions that are split into their xy- and z-polarized components and one higher energy state). Fitting parameters are given in Table 4.*

We then adjusted our synthetic methods to try and obtain higher quality, more monodisperse NCs, as given in Appendix II. [24] Working with small adjustments to the concentration of precursors, temperature of precursor injection, and type of phosphine ligand, we were able to obtain NCs that had their first absorption maximum at 522, 538, 551, and 613 nm prior to ligand exchange. These NCs were deemed as higher quality and more monodispersed based upon a sharper, more distinct second transition in the absorption, higher photoluminescence quantum yields, and narrower absorption and emission spectra. Upon completion of ligand exchange, these corresponded to NCs with diameters of 2.8, 3.0, 3.2, and 5.2 nm respectively.[25] This second set of highly monodisperse nanocrystals gave small

differences in Raman cross sections, but lower overtone to fundamental ratios and depolarization ratios. We believe that this was due to the elimination of smaller NCs that may be on resonance with higher energy excitations.

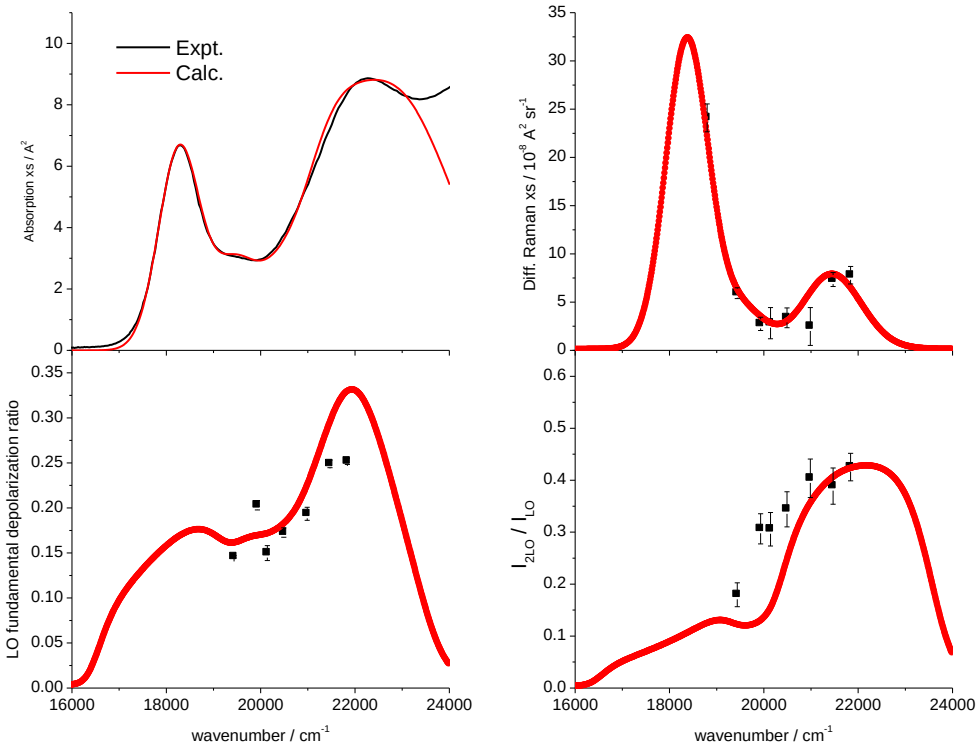


*Figure 18. Same as Fig. 17 (four xy/z pairs and one higher energy state) but for NCs 3.0 nm in diameter. Parameters of the model are given in Table 4.*

The resonance Raman depolarization ratios are particularly sensitive to the polarizations of the underlying electronic transitions.[17] For a spherical oscillator, the Raman depolarization ratio is zero for totally symmetric vibrations. If the excitation is resonant with a single, linearly polarized excitation (linear oscillator), then $\rho = 1/3$; a xy degenerate transition (planar oscillator) gives $\rho = 1/8$. We measured depolarization ratios that were much greater than zero which indicates that our NCs optical properties are far from spherically symmetric. Our original studies showed depolarization ratios very close to $\rho = 1/3$ in the higher energy spectral region and approach those for a linear oscillator.[7] Therefore we only included the z-polarized component in our modeling parameters for that region. Our final NCs however had smaller depolarization ratios and required the xy- and z- polarized components for the higher energy region in order to fit the data. The results of EPC for our areas of interest are given in Table 3 (the areas of interest being the first excitonic peak and the higher energy spectral region approximately 2000-5000 cm$^{-1}$ above the first

exciton). As one can see, our data shows that there is relatively no size dependence for the amount of EPC for the lowest-energy exciton while the higher energy spectral region contains multiple components, one or more transitions that have a small contribution to the amount of EPC and another with a large contribution to the amount of EPC.

Figures 17-19 and Table 4 give the fitting parameters for each sized NC where each NC could be fit to the same Huang-Rhys parameter. From previously reported literature, [54] we know that the energy spacing between transitions becomes larger as one decreases the particle diameter. Our results clearly indicate this trend by observing the spacing between the first and second transitions (the $1S_{3/2}$-$1S_e$ and $2S_{3/2}$-$1S_e$) increase with decreasing NC size (755, 1090, 1140, 1165 $cm^{-1}$ for NCs that are 5.2, 3.2, 3.0, and 2.8 nm respectively). Furthermore, the spacing between the xy- and z-polarized components clearly increase with decreasing NC size (100, 150, 190, 200 $cm^{-1}$ for NCs that are 5.2, 3.2, 3.0, and 2.8 nm diameters respectively); however to an extent, these parameters fall out of assumptions made from Reference 54 and when deciding how to vary the parameters to best fit the data.

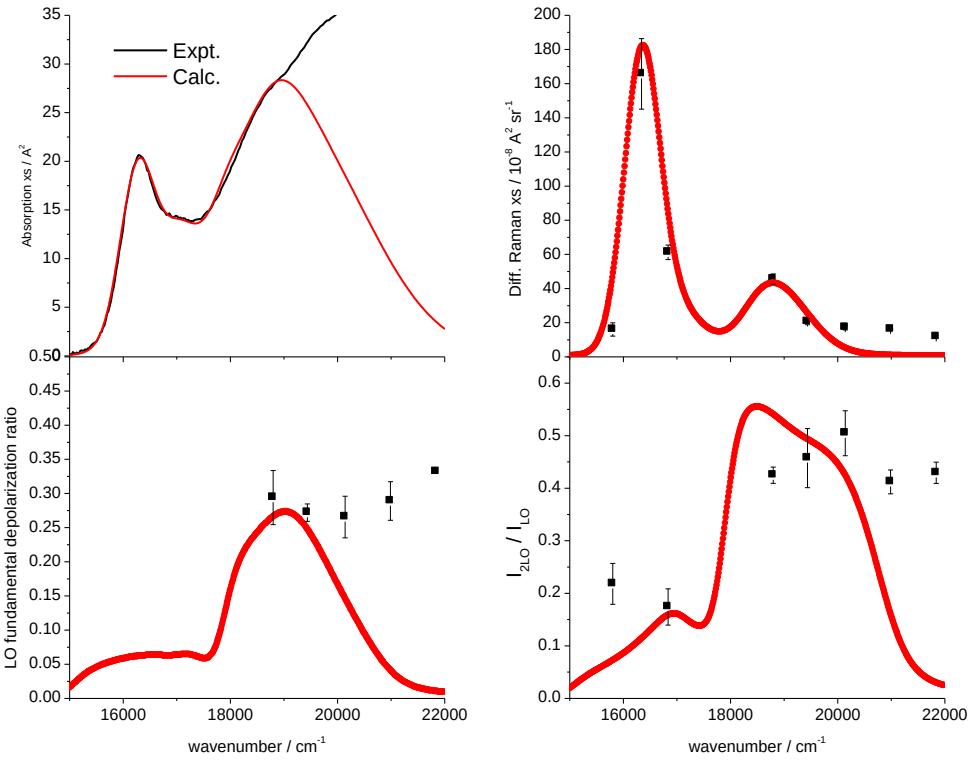


*Figure 19. Same as Fig. 17 (four xy/z pairs and one higher energy state) but for NCs 5.2 nm in diameter. Parameters of the model are given in Table 4. Large deviations from experiment for the highest energy excitations are due a lack of trying to fit the data in this high energy region (beyond the first 9-transitions).*

*Table 4. Summary of fitting parameters for various sized nanocrystals. Listed frequencies (from top to bottom of each transition) are for particles that absorb about 613, 557, 545, and 528 nm (that correspond to NCs with 5.2, 3.2, 3.0, and 2.8 nm diameters respectively). Inhomogeneous widths were 707, 918, 965, and 1013 $cm^{-1}$ (FWHM) respectively. Splitting between xy and z polarized components of the first three transitions: 100, 150, 190, and 200 $cm^{-1}$ respectively.*

| center frequency / $cm^{-1}$ | homogeneous width (FWHM) / $cm^{-1}$ | transition length / Å | polarization | S | assignment [ref. 32] |
|---|---|---|---|---|---|
| 16235 | 250 | 2.17 | xy | 0.08 | $1S_{3/2}1S_e$ |
| 17890 | 250 | 1.55 | | 0.08 | |
| 18210 | 280 | 1.44 | | 0.08 | |
| 18845 | 310 | 1.32 | | 0.08 | |
| 16335 | 250 | 2.17 | z | 0.08 | |
| 18040 | 250 | 1.55 | | 0.08 | |
| 18400 | 280 | 1.44 | | 0.08 | |
| 19045 | 310 | 1.32 | | 0.08 | |
| 16990 | 260 | 1.35 | xy | 0.06 | $2S_{3/2}1S_e$ |
| 18980 | 270 | 0.86 | | 0.08 | |
| 19350 | 300 | 0.84 | | 0.08 | |
| 20010 | 340 | 0.75 | | 0.08 | |
| 17090 | 260 | 1.35 | z | 0.06 | |
| 19130 | 270 | 0.86 | | 0.08 | |
| 19540 | 300 | 0.84 | | 0.08 | |
| 20210 | 340 | 0.75 | | 0.08 | |
| 17845 | 300 | 0.95 | xy | 0.06 | $1S_{1/2}1S_e$ (?) |
| 19940 | 300 | 0.56 | | 0.08 | |
| 20225 | 300 | 0.55 | | 0.08 | |
| 21015 | 350 | 0.69 | | 0.08 | |
| 17945 | 300 | 0.95 | z | 0.06 | |
| 20090 | 300 | 0.56 | | 0.08 | |
| 20415 | 300 | 0.55 | | 0.08 | |
| 21215 | 350 | 0.69 | | 0.08 | |
| 18635 | 375 | 1.56 | xy | 1.53 | $1P_{3/2}1P_e$ |
| 21275 | 400 | 1.05 | | 1.53 | |
| 21275 | 415 | 0.87 | | 0.78 | |
| 22220 | 550 | 0.81 | | 0.72 | |
| 19135 | 375 | 1.56 | z | 1.53 | |
| 21775 | 400 | 1.05 | | 1.53 | |
| 21775 | 415 | 0.87 | | 0.78 | |
| 22720 | 550 | 0.81 | | 0.72 | |
| 19200 | 3000 | 7.82 | z | 0 | ??? |
| 22025 | 3000 | 4.45 | | 0 | |
| 22635 | 3000 | 4.42 | | 0 | |
| 23825 | 3300 | 4.15 | | 0 | |

Additionally, both homogeneous and inhomogeneous widths increase with decreasing NC size. This could be accounted for based on the amount of nucleation and growth of each NC. When synthesizing smaller NCs, we use a higher injection temperature to obtain more nuclei and therefore the starting materials are used at a much faster rate. Due to the quickness of these reactions, this causes one to have more inhomogeneity as well as homogeneous broadening within the NCs. One can also clearly see that for the two main areas of interest, the first exciton and the higher energy spectral region, the transition length increases with increasing NC size, as can be seen in Table 4. This result however, isn't something that comes out of our fitting but rather, something that is assumed when using the relationships between the excitonic absorption peak and extinction coefficient in Reference 25. Therefore, this result may not follow when using another method to determine the extinction coefficient.

Lastly, the transition we label as $1S_{1/2}$-$1S_e$ in Table 4, is the one transition that didn't follow with any smooth, monotonic trends with regards to transition length. This could possibly be explained by Reference 60, which stated that the relative intensities for some transitions are strongly dependent on NC size. In figure 4 of Reference 60, they show how some transitions, the $1S_{1/2}$-$1S_e$ for instance, only appear in the spectrum of some sizes of NCs, but not all. This finding could account for the large variation between the transition lengths of this particular transition while we were able to obtain constant or monotonic trends for all of our other data.

## Discussion

Originally, this project was to determine the amount of electron-phonon coupling (via the Huang-Rhys parameter) for CdSe NCs. Due to the sensitivities to other factors, like the homogeneous broadening, the Huang-Rhys parameter can only be determined within a range that depends on a few assumptions. Once the experimental absorption cross-section is used to fix the transition dipole moment, the LO fundamental Raman cross-section depends on a combination of the Huang-Rhys factors and the homogeneous broadening. As mentioned above in Figures 12 and 13, the values for the Huang-Rhys parameter (S) can range from less than 0.01 to about 1. However, when one considers the overtone to fundamental ratio, depolarization ratio, and the emission stokes shift, this further narrows the acceptable range of S where we found a best fit value of about 0.08 across all NC sizes. One thing to note is that reasonable fits can be obtained with S ranging from 0.04 to 0.15, which are in good agreement with References 54 and 55, while others have experimental values that are smaller [14,41] and larger [11,15,38-40] than ours.

Quantitative analysis of Raman excitation profiles requires knowledge of the molar absorptivity in order to determine the concentration of the CdSe NCs in the sample which is then used to calculate the experimental Raman cross sections using Eq. (6). Several groups have experimentally determined molar absorptivities for CdSe NCs as a function of size.[25,56-59] One finds there is considerable spread among the different values. In order to evaluate the heartiness of our modeling results, we repeated the analysis using the molar absorptivities reported by Ref. 56 on our 3.2 nm NCs, which are nearly a factor of two smaller than the values from the Mulvaney group [25] originally used. While the best-fit transition moments, linewidths, and Huang-Rhys factors all change to some extent, the qualitative conclusions still hold: the low-lying excitations have small EPC ($S<0.25$) while the higher-energy absorption arises from a combination of transitions, some with very weak ($S < 0.1$) and others with strong ($S > 1$) EPC.

Our initial EPC size dependent study was similar to that of our previous group work in that NC polydispersion can cause an increase in the Raman cross sections at higher energies due to increased contributions from smaller NCs lowest excitonic transitions. Adjusting ones synthetic methods to obtain highly monodispersed and highly luminescent NCs allows for more accurate data as seen in our final size dependent results.

Our results indicate that there is no size dependence on EPC across the first three transitions in our CdSe NCs as seen in Table 4. This result may not be surprising because these NCs are in the strong confinement limit and therefore may exhibit similar EPC strengths. In addition, it is known that the EPC increases as size increases (bulk CdSe has S~10),[15,52,61] however it is not clear how large NCs have to be for there to be an increase of the Huang-Rhys parameter.

In contrast, our results indicate that the higher energy spectral region, typically assigned as $1P_{3/2}1P_e$ transition, consists of multiple overlapping transitions where

most of the oscillator strength is carried by transitions having very little EPC, while another component has little oscillator strength and strong EPC across all of our NC sizes. The transition that is composed of little oscillator strength and strong EPC does seem to show smaller transition lengths and smaller Huang-Rhys parameters as NC size decreases. Furthermore, the calculations of Efros and Rosen [31] predict that while $1P_{3/2}1P_e$ is the strongest transition in this region, it has only about the same, or smaller, oscillator strength as $1S_{3/2}1S_e$, consistent with the assignments made in Table 4. The remaining absorbance in this region must arise from other transitions with no Raman contribution and it is not clear whether these are other delocalized excitonic transitions or, possibly, surface states.

## Conclusions

Our resonance Raman excitation profile studies completed on NCs with 2.8, 3.0, 3.2, and 5.2 nm, wurtzite form, organically capped CdSe nanocrystals in room temperature chloroform solvent yielded the following conclusions:

1. Inhomogeneous broadening and homogeneous broadening make comparable contributions to the observed width of ~1000 $cm^{-1}$ for the lowest-energy excitonic transition.
2. The excitonic transitions become more nearly linearly polarized at higher excitation energies.
3. The Huang-Rhys factor for the $1S_{3/2}$-$1S_e$ lowest energy excitonic transition is in the range S=0.04–0.15, with a best fit of S=0.08 for all NC sizes.
4. The higher energy spectral region between 2000 and 5000 $cm^{-1}$ above the lowest-energy transition contains multiple excitonic transitions: one or more of these transitions has a large oscillator strength and makes a negligible contribution to the resonance Raman intensity, probably because of very weak EPC or very rapid electronic dephasing while one or more transitions has a small amount of oscillator strength and large Huang-Rhys factors.

## References


1. Kelley, A. M. (2010). Electron – Phonon Coupling in CdSe Nanocrystals. *J. Phys. Chem. Lett., 1 (9)*, 1296.
2. Klimov, V. I. (2006). Mechanisms for Photogeneration and Recombination of Mulitexciton in Semiconductor Nanocrystals: Implications for Lasing and Solar Energy Conversion. *J. Phys. Chem. B., 110,* 16827.
3. Wheeler, D. A. and Zhang, J. Z. (2013). Exciton Dynamics in Semiconductor Nanocrystals. *Adv. Mater. 25 (21),* 2878-2896
4. "Core-Shell Semiconductor Nanocrystal," Retrieved from http://en.wikipedia.org/wiki/Core%E2%80%93shell_semiconductor_nanocrystal, Last accessed 6/24/13
5. Kuno, M. (2012) *Introductory Nanoscience Physical and Chemical Concepts*, New York, NY: Garland Science.
6. Jiang, Z. and Kelley, D. F., (2010). Role of Surface States in the Exciton Dynamics of Core and Core/Shell Nanorods. *J. Phys. Chem. C 114 (41),* 17519.
7. Baker, J. A., Kelley, D. F., and Kelley, A. M. (2013). Resonance Raman and Photoluminescence Excitation Profiles and Excited-state Dynamics in CdSe Nanocrystals. *J. Chem. Phys. 139,* 024702.
8. Kelley, A. M. (2008). Resonance Raman and Resonance Hyper-Raman Intensities: Structure and Dynamics of Molecular Excited States in Solution. *J. Phys. Chem. A 112 (47),* 11975.
9. Myers, A. B. (1995). *Laser Techniques in Chemistry, edited by A. B. Myers and T. R. Rizzo*, New York, NY: Wiley.
10. Myers, A. B. and Mathies, R. A. (1987). *Biological Applications of Raman Spectroscopy, edited by T. G. Spiro*, New York, NY: Wiley
11. Baranov, A. V., Rakovich, Y. P., Donegan, J. F., Perova, T. S., Moore, R. A., Talapin, D. V., Rogach, A. L., Masumoto, Y., and Nabiev, I. (2003). Effect of ZnS Shell Thickness on the Phonon Spectra in CdSe Quantum Dots, *Phys. Rev. B 68 (16),* 165306.
12. Lange, H., Artemyev, M., Woggon, U., Niermann T., and Thomsen, C. (2008). Expimental Investigation of the exciton-LO phonon coupling in CdSe/ZnS core/shell nanorods, *Phys. Rev. B 77 (19),* 193303.
13. Dzhagan, V. M., Valakh, M. Y., Raevskaya, A. E., Stroyuk, A. L., Kuchmiy, S. Y., and Zahn, D. R. T. (2008). Size Effects on Raman Spectra of Small CdSe Nanoparticles in Polymer Films, *Nanotechnology 19,* 305707.
14. Sagar, D. M., Cooney, R. R., Sewall, S. L., Dias, E. A., Barsan, M. M., Butler, I. S., and Kambhampati, P. (2008). Size Dependent, State-Resolved Studies of Exciton-Phonon Couplings in Strongly Confined Semiconductor Quantum Dots, *Phys. Rev. B 77,* 235321.

15. Alivisatos, A. P., Harris, T. D., Carroll, P. J., Steigerwald, M. L., and Brus, L. E. (1989). Electron-Vibration Coupling in Semiconductor Clusters by Resonance Raman Spectroscopy, *J. Chem. Phys. 90,* 3463.
16. Shiang, J. J., Craig, I. M., and Alivisatos, A. P. (1993). Resonance Raman Depolarization Ratios in CdSe Nanocrystals, *Z. Phys. D 26,* 358.
17. Shiang, J. J., Kadavanich, A. V., Grubbs, R. K., and Alivisatos, A. P. (1995). Symmetry of Annealed Wurtzite CdSe Nanocrystals: Assignment of the $C_{3v}$ Point Group, *J. Phys. Chem. 99 (48),* 17417.
18. Kelley, A. M., Dai, Q., Jiang, Z., Baker, J. A., and Kelley, D. F. (2013). Resonance Raman Sectra of Wurtzite and Zincblende CdSe Nanocrystals, *Chem. Phys. 422,* 272-276.
19. Kelley, A. M. (2011). Electron-Phonon Coupling in CdSe Nanocrystals from an Atomistic Phonon Model. *ACS Nano 5,* 5254.
20. Klein, M. C., Hache, F., Ricard, D., Flytzanis, C. (1990). Size Dependence of Electron-Phonon Coupling in Semiconductor Nanospheres: The Case of CdSe, *Phys. Rev. B. 42,* 11123-11132.
21. Takagahara, T. (1993). Electron-Phonon Interactions and Excitonic Dephasing in Semiconductor Nanocrystals, *Phys. Rev. Lett. 71,* 3577-3580.
22. Salvador, M. R., Graham, M. W., and Scholes, G. D. (2006). Exciton-Phonon Coupling and Disorder in the Excited States of CdSe Colloidal Quantum Dots, *J. Chem. Phys. 125,* 184709.
23. Jiang, Z. and Kelley, D. F. (2011). Surface Charge and Piezoelectric Fields Control Auger Recombination in Semiconductor Nanocrystals, *Nano Lett. 11 (10),* 4067.
24. Gong, K., Zeng, Y., and Kelley, D.F. (2013) Extinction Coefficients, Oscillator Strengths, and Radiative Lifetimes of CdSe, CdTe, and CdTe/CdSe Nanocrystals, *J. Phys. Chem. C. 117 (39),* 20268-20279.
25. Jasieniak, J., Smith, L., van Embden, J., Mulvaney, P., and Califano, M. (2009). Re-examination of the Size-Dependent Absorption Properties of CdSe Quantum Dots, *J. Phys. Chem. C 113 (45),* 19468.
26. Foster, C. E., Barham, B. P., and Reid, P. J. (2001). Resonance Raman Intensity Analysis of Chlorine Dioxide Dissovled in Chloroform: The Role of Nonpolar Solvation, *J. Chem. Phys. 114,* 8492.
27. Wuister, S. F., de Mello Donegá, C., and Meijerink, A. (2004). Influence of Thiol Capping on the Exciton Luminescence and Decay Kinetics of CdTe and CdSe Quantum Dots, *J. Phys. Chem. B 108 (45),* 17393.
28. Klimov, V. I. (2007).Spectral and Dynamical Properties of Mulitexcitons in Semiconductor Nanocrystals, *Ann. Rev. Phys. Chem. 58*, 635.
29. Efros, A.L., Rosen, M., Kuno, M., Nirmal, M., Norris, D.J., and Bawendi, M. (1996). Band-Edge Exciton in Quantum Dots of Semiconductors with a Degenerate Valence Band: Dark and Bright Exciton States, *Phys. Rev. B 54,* 4843.

30. Li, J. and Wang, L. (2003). High Energy in Excitons in CdSe Quantum Rods, *Nano Lett. 3 (1)*, 101.
31. Efros, A. L. and Rosen, M. (2000). The Electronic Structure of Semiconductor Nanocrystals, *Ann. Rev. Mater. Sci. 30*, 475.
32. Norris, D. J. and Bawendi, M. G. (1996). Measurement and Assignment of the Size-Dependent Optical Spectrum in CdSe Quantum Dots, *Phys. Rev. B 53,* 16338.
33. Wang, L.-W. and Zunger, A. (1998). High-Energy Excitonic Transitions in CdSe Quantum Dots, *J. Phys. Chem. B 102 (34)*, 6449.
34. Htoon, H., Cox, P. J., and Klimov, V. I. (2004). Structure and Excited-State Transitions of Individual Semiconductor Nanocrystals Probed by Photoluminescence Excitation Spectroscopy, *Phys. Rev. Lett. 93*, 187402.
35. Chilla, G., Kipp, T., Menke, T., Heitmann, D., Nikolic, M., Fromsdorf, A., Kornowski, A., Forster, S., and Weller, H. (2008). Direct Observation of Confined Acoustic Phonons in the Photoluminescence Spectra of a Single CdSe-CdS-ZnS Core-Shell-Shell Nanocrystal, *Phys. Rev. Lett. 100*, 057403.
36. Fernée, M. J., Littleton, B. N., Cooper, S., Rubinsztein-Dunlop, H., Gomez, D. E., and Mulvaney, P. (2008). Acoustic Phonon Contributions to the Emission Spectrum of Single CdSe Nanocrystals, *J. Phys. Chem. C 112 (6),* 1878.
37. Empedocles, S. A., Norris, D. J., and Bawendi, M. G. (1996). Photoluminescence Spectroscopy of Single CdSe Nanocrystallite Quantum Dots, *Phys. Rev. Lett. 77,* 3873.
38. Groeneveld, E. and de Mello Donegá, C. (2012). Enhanced Exciton-Phonon Coupling in Colloidal Type-II CdTe-CdSe Heteronanostructures, *J. Phys. Chem. C 116 (30),* 16240.
39. McKimmie, L. J., Lincoln, C. N., Jasieniak, J., and Smith, T. A. (2010). Three-Pulse Photon Echo Peak Shift Measurements of Capped CdSe Quantum Dots, *J. Phys. Chem. C 114 (1),* 82.
40. Mittleman, D. M., Schoenlein, R. W., Shiang, J. J., Colvin, V. L., Alivisatos, A. P., and Shank, C. V. (1994). Quantum Size Dependence of Femtosecond Electronic Dephasing and Vibrational Dynamics in CdSe Nanocrystals, *Phys. Rev. B 49,* 14435.
41. Sagar, D. M., Cooney, R. R., Sewall, S. L., and Kambhampati, P. (2008). State-Resolved Exciton-Phonon Couplings in CdSe Semiconductor Quantum Dots, *J. Phys. Chem. C 112 (25),* 9124.
42. Tschirner, N., Lange, H., Schliwa, A., Bierman, A., Thomsen, C., Lambert, K., Gomes, R., and Hens, Z. (2012). Interfacial Alloying in CdSe/CdS Heteronanocrystals: A Raman Spectroscopy Analysis, *Chem. Mater. 24 (2)*, 311.
43. Lin, C., Kelley, D. F., Rico, M., and Kelley, A. M. (2014). The "Surface Optical" Phonon in CdSe Nanocrystals, *ACS Nano 8 (4)*, 3928.
44. Myers, A. B. (1998). Molecular Electronic Spectral Broadening in Liquids and Glasses, *Ann. Rev. Phys. Chem. 49,* 267.

45. Salvador, M. R., Hines, M. A., and Scholes, G. D. (2003). Exciton-Bath Coupling and Inhomogeneous Broadening in the Optical Spectroscopy of Semiconductor Quantum Dots, *J. Chem. Phys. 118,* 9380.
46. Biadala, L., Louyer, Y., Tamarat P., and Lounis, B. (2009). Direct Observation of the Two-Lowest Exciton Zero-Phonon Lines in Single CdSe/ZnS Nanocrystals, *Phys. Rev. Lett. 103,* 037404.
47. Myers, A. B. and Li, B. (1990). Resonance Raman Quantum Yields for $CS_2$ in Solution: Dyanmics of Solvent-Induced Spectral Broadening, *J. Chem. Phys. 92*, 3310.
48. Phillips, D. L. and Myers, A. B. (1991). Photodissociation of alkyl iodides in solution: Substituent effects on the early time dynamics. *J. Chem. Phys. 95*, 226.
49. Sension, R. J. and Strauss, H. L. (1986). Comparison of experiment and theory for the resonance Raman spectrum of $I_2$ in solution. I. The Raman excitation profile of $I_2$ in n-hexane. *J. Chem. Phys. 85*, 3791.
50. Kelley, A.M. (2013) *Condensed Phase Molecular Spectroscopy and Photophysics*, Hoboken, NJ: John Wiley & Sons.
51. Mukamel, S. (1995) *Principles of Nonlinear Optical Spectroscopy*, New York, NY: Oxford University Press.
52. Merlin, R., Güntherodt, G. Humphreys, R. Cardona, M. Suryanarayanan, R. and Holtzerg, F. (1978). Multiphonon process in YbS. *Phys. Rev. B 17*, 4951.
53. Kulinowski, K., Gould, I. R., and Myers, A. B., (1995). Absorption, Fluorescence and Resonance Raman Spectroscopy of the Hexamethylbenzene/ Tetracyanoethylene Charge-Transfer Complex: Toward a Self-Consistent Model. *J. Phys. Chem. 99*, 9017.
54. Norris, D. J., Efros, A. L., Rosen, M., and Bawendi, M. G. (1996). Size Dependence of Exciton Fine Structure in CdSe Quantum Dots. *Phys. Rev. B 53*, 16347.
55. Salvador, M. R., Graham, M. W., and Scholes, G. D. (2006). Exciton-phonon coupling and disorder in excited states of CdSe colloidal quantum dots. *J. Chem. Phys. 125*, 184709.
56. Yu, W. W., Qu, L., Guo, W., and Peng, X. (2003). Experimental Determination of the Extinction Coefficient of CdTe, CdSe, and CdS Nanocrystals. *Chem. Mat. 15*, 2854.
57. Leatherdale, C. A., Woo, W.-K., Mikulec, F. V., and Bawendi, M. G. (2002). On the Absorption Cross Section of CdSe Nanocrystal Quantum Dots. *J. Phys. Chem. B 106*, 7619.
58. de Mello Donegá, C. and Koole, R. (2009). Size Dependence of the Spontaneous Emission Rate and Absorption Cross Section of CdSe and CdTe Quantum Dots. *J. Phys. Chem. C 113*, 6511.
59. Capek, R. K., Moreels, I., Lambert, K., De Muynck, D., Zhao, Q., Van Tomme, A., Vanhaecke, F., and Hens, Z. (2010). Optical Properties of Zincblende Cadmium Selenide Quantum Dots. *J. Phys. Chem. C 114*, 6371.

60. Ekimov, A. I., Hache, F., Schanne-Klein, M. C., Ricard, D., Flytzanis, C., Kudryavtsev, I. A., Yazeva, T. V., Rodina, A. V., and Efros, A. L. (1993). Absorption and Intensity Dependent Photoluminescence Measurements on CdSe Quantum Dots: Assignment of the First Electronic Transitions. *J. Opt. Soc. Am. B 10*, 100.
61. Gross, E., Permogorov, S., Morozenko, Ya., and Kharlmov, B. (1973). Hot-Exciton Luminescence in CdSe Crystals. *Physica Status Solidi B 59*, 551
62. Fredrick, M. T., Amin, V. A., Cass, L. C., and Weiss, E. A. (2011). A Molecule to Detect and Perturb the Confinement of Charge Carriers in Quantum Dots. *Nano Lett. 11*, 5455.

## Appendix I – Traditional Synthetic Procedure of CdSe

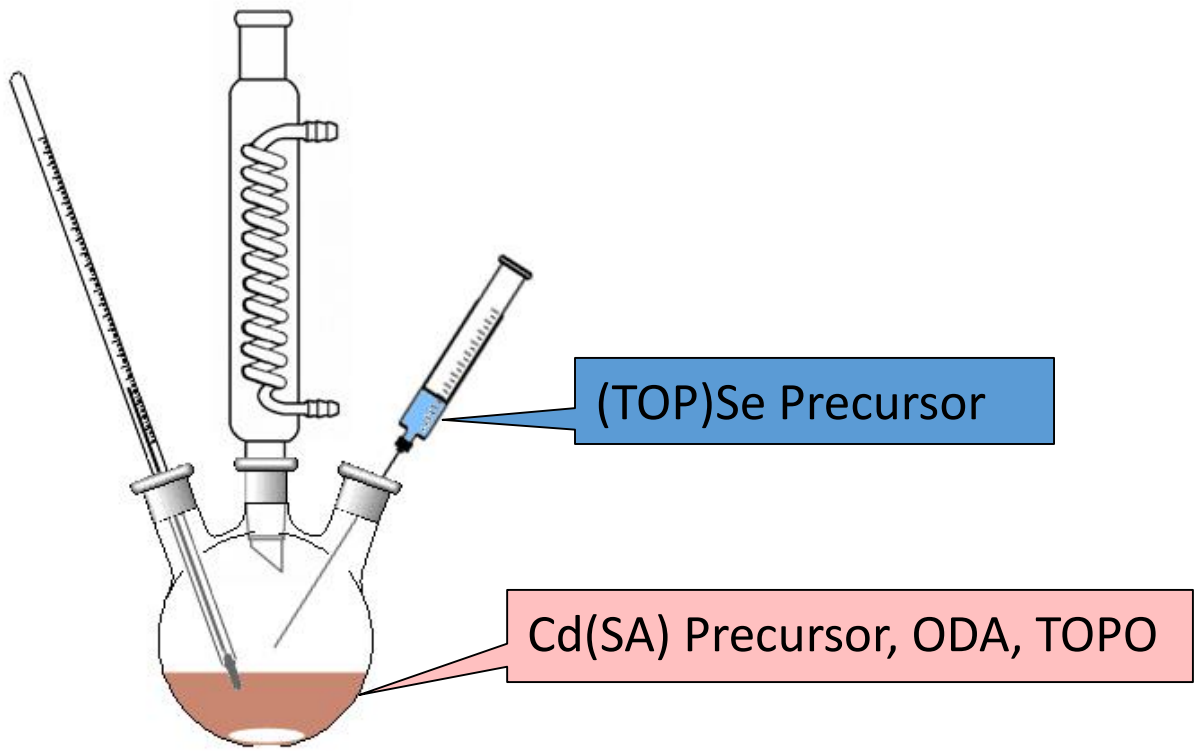


*Figure 20, Reaction vessel of CdSe nanocrystals in octadecene. Photo reproduced courtesy of Dr. Chen Lin*

Cd(SA) Precursor
0.4 mmol Cadmium Oxide (CdO)
1.6 mmol Steric Acid (SA)
5.5 mL Octadecene (ODE)

(TOP)Se Precursor
2 mmol Selenium (Se)
4.5 mmol Trioctylphosphine (TOP)
3.5 mL ODE

Part I – Precursor Preparation
In a medium to large vial, combine 2 mmol Se, 3.5 mL ODE, and a stir bar. Cap vial with a septum stopper and degas using nitrogen. Place vial in glovebox and add 4.5 mmol TOP. Allow this precursor to react under stirring until all the Se is dissolved. Set aside for use once Cd(SA) precursor is ready.

In a three-necked flask, combine 0.4 mmol CdO, 1.6 mmol SA, 5.5 mL ODE, and a stir bar. Use a septum stopper to seal one neck, a thermocouple to seal a second, and a condenser WITH a septum stopper and 16 gauge needle on top but WITHOUT water flow to seal the third. Heat and stir this reaction vessel to about 250° C under a very small nitrogen flow and allow to react until a colorless solution is obtained, typically 45-60 minutes. Allow to cool to room temperature, add 3.0 g octadecylamine (ODA) and 1.0 g trioctylphosphine oxide (TOPO). Heat quickly to 280° C.

Part II – The Reaction

To inject (TOP)Se precursor rapidly, draw precursor solution into a 10 mL syringe with a short 16 gauge needle making sure to only draw solution and not any air. Inject (TOP)Se rapidly into Cd(SA) solution immediately once the reaction reaches 280°C. Allow to react at about 250° C and stop reaction at desired sized particles (approximately 20-30 seconds) by decreasing reaction temperature below 200° C. When reaction reaches 100° C add about 5 mL of toluene. Place reaction solution into vial or flask and seal with a septum stopper. Degas using nitrogen and store for further use.

Part III – Purification

Obtain a 1-2 mL aliquot of bulk reaction solution. Add a 50:50 methanol:toluene blend to precipitate particles. Centrifuge for approximately 30 seconds, just long enough for the particles to fall out of solution but keep any remaining unreacted reactants in solution. Pour off the supernatant and add about 1-2 mL of toluene. Repeat the purification procedure until one obtains an optically clear solution.

## Appendix II – New Size Focused Synthesis of CdSe

Small Nanocrystals (<3 nm)

Cd(SA) Precursor
0.4 mmol CdO
2.4 mmol SA
5.5 mL ODE

(TOP)Se Precursor
0.8 mmol Se
0.96 mmol TOP
1.5 mL ODE

Part I – Precursor Preparation
In a medium to large vial, combine 0.8 mmol Se, 1.5 mL ODE, and a stir bar. Cap vial with a septum stopper and degas using nitrogen. Place vial in glovebox and add 0.96 mmol TOP. Allow this precursor to react under stirring until all the Se is dissolved. Set aside for use once Cd(SA) precursor is ready.

In a three-necked flask, combine 0.4 mmol CdO, 2.4 mmol SA, 5.5 mL ODE, and a stir bar. Use a septum stopper to seal one neck, a thermocouple to seal a second, and a condenser WITH a septum stopper and 16 gauge needle on top but WITHOUT water flow to seal the third. Heat and stir this reaction vessel to about 250° C under a very small nitrogen flow and allow to react until a colorless solution is obtained, typically 45-60 minutes. Allow to cool to room temperature, add 2.0 g ODA and 0.7 g TOPO. Heat quickly to 295° C.

Part II – The Reaction

To inject (TOP)Se precursor rapidly, draw precursor solution into a 10 mL syringe with a short 16 gauge needle making sure to only draw solution and not any air. Inject (TOP)Se rapidly into Cd(SA) solution immediately once the reaction reaches 295°C and lower the heating mantle immediately. Allow to react at about 250° C and stop reaction at desired size by decreasing reaction temperature below 200° C. Note: it will take approximately 45-60 seconds for the particles to fully develop. When reaction reaches 100° C add about 5 mL of toluene. Place reaction solution into vial or flask and seal with a septum stopper. Degas using nitrogen and store for further use.

Part III – Purification

Obtain a 1-2 mL aliquot of bulk reaction solution. Add a 50:50 methanol:toluene blend to precipitate particles. Centrifuge for approximately 30 seconds, just long enough for the particles to fall out of solution but keep any remaining unreacted reactants in solution. Pour off the supernatant and add about 1-2 mL of toluene. Repeat the purification procedure until one obtains an optically clear solution.

Medium Nanocrystals (3-3.5 nm)

Cd(SA) Precursor
0.4 mmol CdO
2.4 mmol SA
5.0 mL ODE

(TOP)Se Precursor
1.6 mmol Se
1.92 mmol TOP
1.0 mL ODE

Part I – Precursor Preparation

In a medium to large vial, combine 1.6 mmol Se, 1.0 mL ODE, and a stir bar. Cap vial with a septum stopper and degas using nitrogen. Place vial in glovebox and add 1.92 mmol TOP. Allow this precursor to react under stirring until all the Se is dissolved. Set aside for use once Cd(SA) precursor is ready.

In a three-necked flask, combine 0.4 mmol CdO, 2.4 mmol SA, 5.0 mL ODE, and a stir bar. Use a septum stopper to seal one neck, a thermocouple to seal a second, and a condenser WITH a septum stopper and 16 gauge needle on top but WITHOUT water flow to seal the third. Heat and stir this reaction vessel to about 250° C under a very small nitrogen flow and allow to react until a colorless solution is obtained, typically 45-60 minutes. Allow to cool to room temperature, add 2.0 g ODA and 0.7 g TOPO. Heat quickly to 285° C.

Part II – The Reaction

To inject (TOP)Se precursor rapidly, draw precursor solution into a 10 mL syringe with a short 16 gauge needle making sure to only draw solution and not any air. Inject (TOP)Se rapidly into Cd(SA) solution immediately once the reaction reaches 285°C. Allow to react at about 250° C and stop reaction at desired sized particles (approximately 60-120 seconds) by decreasing reaction temperature below 200° C. When reaction reaches 100° C add about 5 mL of toluene. Place reaction solution into vial or flask and seal with a septum stopper. Degas using nitrogen and store for further use.

Part III – Purification

Obtain a 1-2 mL aliquot of bulk reaction solution. Add a 50:50 methanol:toluene blend to precipitate particles. Centrifuge for approximately 30 seconds, just long enough for the particles to fall out of solution but keep any remaining unreacted reactants in solution. Pour off the supernatant and add about 1-2 mL of toluene. Repeat the purification procedure until one obtains an optically clear solution.

Large Nanocrystals (>3.5 nm)

Cd(OA) Precursor

0.2 mmol CdO
1.2 mmol Oleic Acid (OA)
6.0 mL ODE

(TOP)Se Precursor

1.0 mmol Se
1.5 mmol Tributylphosphine (TBP)
1.0 mL ODE

Part I – Precursor Preparation

In a medium to large vial, combine 1.0 mmol Se, 1.0 mL ODE, and a stir bar. Cap vial with a septum stopper and degas using nitrogen. Place vial in glovebox and add 1.5 mmol TBP. Allow this precursor to react under stirring until all the Se is dissolved. Set aside for use once Cd(OA) precursor is ready.

In a three-necked flask, combine 0.2 mmol CdO, 1.2 mmol OA, 6.0 mL ODE, and a stir bar. Use a septum stopper to seal one neck, a thermocouple to seal a second, and a condenser WITH a septum stopper and 16 gauge needle on top but WITHOUT water flow to seal the third. Heat and stir this reaction vessel to about 250° C under a very small nitrogen flow and allow to react until a colorless solution is obtained, typically 45-60 minutes. Allow to cool to room temperature, add 1.0 g ODA and 0.5 g TOPO. Heat quickly to 280° C.

Part II – The Reaction

To inject (TBP)Se precursor rapidly, draw precursor solution into a 10 mL syringe with a short 16 gauge needle making sure to only draw solution and not any air. Inject (TBP)Se rapidly into Cd(OA) solution immediately once the reaction reaches 280°C. Allow to react at about 255° C and stop reaction at desired sized particles (approximately 60-120 seconds) by decreasing reaction temperature below 200° C. When reaction reaches 100° C add about 5 mL of toluene. Place reaction solution into vial or flask and seal with a septum stopper. Degas using nitrogen and store for further use.

Part III – Purification

Obtain a 1-2 mL aliquot of bulk reaction solution. Add a 50:50 methanol:toluene blend to precipitate particles. Centrifuge for approximately 30 seconds, just long enough for the particles to fall out of solution but keep any remaining unreacted reactants in solution. Pour off the supernatant and add about 1-2 mL of toluene. Repeat the purification procedure until one obtains an optically clear solution.

## Appendix III – Computational Fortran Code

### Provided by: Dr. Anne Myers Kelley

```
program ncrrep
c
c     Program to calculate Raman and absorption intensities using time-dep
c     method with up to ten excited electronic states treated in the simple harmonic
c          limit.  Each excited state may be either z or xy polarized.
c     Two vibrational modes may be coupled to either or both transitions.
c     Each mode is thermally populated up to v = 2.
c     Uses Mukamel's Brownian oscillator model for the solvent induced
c     broadening (identical to stochastic model for real part of broadening
c     function, but with imaginary part which gives solvent Stokes shift).x
c     The formula correct when not in the high temperature limit is used.
c     The relaxed fluorescence spectrum is also calculated.
c
c          Raman intensities are reported in units of differential cross section,
c          (A**2/molecule-sr)*1.e8
c
c          Absorption spectrum is printed in "absorp.txt"
c          Input parameters are printed in "ncrrep.out"
c          Raman profile for line x is printed in "profX.txt"
c     Emission spectrum is printed in "emiss.txt"
c
c     Inputs (read from file "ncrrep.in"):
c     nstate = number of excited states (10 max)
c     nline = # Raman transitions to calculate (10 max)
c     ngroup = # distinguishable Raman lines (near degenerate transitions grouped)
c     ntime = # time steps in Fourier transform (5000 max)
c     cutoff = cutoff parameter in the sum over n in Brownian oscillator
c     calc, usually 10-6 to 10-8 range (check convergence by
c     reducing cutoff and re-running)
c     ev(i) = electronic vertical transition energy for state i
c     gamma(i) = electronic homogeneous linewidth (FWHM in cm-1) in state i
c     rkappa(i) = lineshape parameter in stochastic model for state i
c     sig = electronic inhomogeneous width (Gaussian standard dev. in cm-1)
c     u(i) = electronic transition length (A) for state i
c     ipol(i) = polarization of state i, 0 for z and 1 for xy (degenerate)
c     alow,ahigh = lowest and highest energies to calc. absorption
c     elow = lowest energy to calc. emission
c     delt = time step in Fourier transform (fs), typically around 0.5
c     refrac = solvent refractive index
c     wg(j) = vib. freq (cm-1) of mode j
c     delta(i,j) = dimensionless displacement of mode j in state i
```

```
c     temp = temperature in Kelvin
c     nquanta(i,j) = # of quanta excited in mode j in Raman line i
c
      implicit complex (c)
      dimension wg(2),delta(10,2),covlp(10,2,3,3,5000),ceiwt(10,5000)
      dimension ev(10),reorg(10),
     1  cat(10,5000),cgt(5000),toverh(5000),rrpar(1000,10),
     2  csum(10),rrper(1000,10),addpar(1000),addper(1000),igroup(10)
      dimension xfreq(1000),nquanta(10,2),cdamp(10,5000),
     1  xs(1000),ffunc(1000),gfunc(1000),pfunc(501),rashift(10)
      dimension e0(10),gamma(10),rkappa(10),u(10),ipol(10)
      double precision vs(5000),vsi,arg,cutoff,einc,vn,dex,ainc
          character*4 prof,depo,numb(10),ext
      data pi/3.14159/ci/(0.,1.)/hbar/5308.8/
      data xs/1000*0./boltz/0.695/
      data rrper/10000*0./rrpar/10000*0./
          data prof/'prof'/ext/'.txt'/
          data numb/'01','02','03','04','05','06','07','08','09','10'/
c
c     input parameters and print them out
c
      open(unit=30,name='ncrrep.in',type='old')
      open(unit=31,name='ncrrep.out')
      read (30,*) nstate,nline,ngroup,ntime
      if(nline.gt.10) nline=10
          if(ntime.gt.5000) ntime=5000
      read (30,*) sig,cutoff,temp
      write (31,*) ' # time steps, T'
      write (31,*) ntime,temp
          write (31,*) ' Inhom. width, Brownian cutoff'
      write (31,*) sig,cutoff
          do i=1,nstate
                    read (30,*) ev(i),gamma(i),rkappa(i),u(i),ipol(i)
      end do
      write (31,*) ' E vert, gamma, kappa, trans. length, pol.'
          write (31,*) (ev(i),gamma(i),rkappa(i),u(i),ipol(i),i=1,nstate)
      read (30,*) alow,ahigh,elow,delt,refrac
      write (31,*) ' Time step, refractive index'
      write (31,*) delt,refrac
      do i=1,2
            read (30,*) wg(i),(delta(j,i),j=1,nstate)
      end do
      do 40 i=1,nline
 40       read (30,*) (nquanta(i,j),j=1,2),igroup(i)
```

```
      close(unit=30)
           write (31,*) ' frequency, delta in each excited state'
      write (31,*) (wg(i),(delta(j,i),j=1,nstate),i=1,2)
           write (31,*) ' # of quanta in each mode in each line'
           do i=1,nline
                write (31,*) (nquanta(i,j),j=1,2),igroup(i)
                end do
c
c
      pre = 2.08e-20*1.e-6*delt**2*0.3/pi
      delth = delt/hbar
      beta = 1./(boltz*temp)
      do 50 i=1,ntime
 50       toverh(i) = (i-1)*delth
      do j=1,nline
         sh = 0.
         do k=1,2
            kk = nquanta(j,k)+1
                        sh = sh + (kk-1)*wg(k)
         end do
         rashift(igroup(j)) = sh
      end do
      part = 0.
      do n1=0,2
         do n2=0,2
            part = part + exp(-(n1*wg(1)+n2*wg(2))*beta)
         end do
      end do
c
c        Calculate vibrational stuff for each excited state
c        Brownian oscillator first
c
      do 100 l=1,nstate
        do 55 i=1,ntime
 55         vs(i) = 0.
        rk2 = rkappa(l)**2
        a = (2.355+1.76*rkappa(l))/(1.+0.85*rkappa(l)+0.88*rk2)
        rlamb = rkappa(l)*gamma(l)/a
        reorg(l) = beta*(rlamb/rkappa(l))**2/2.
        v = 2.*pi/beta
        n = 0
 510    n = n + 1
        vn = v*n*1.d0
        ainc=vn*delth
```

```
      arg=-1.d0
      einc=dexp(-ainc)
      dex=1.d0
      denom = vn*(vn**2-rlamb**2)
      ii = 0
      do 530 i=2,ntime
        arg = arg+ainc
        dex = dex*einc
        vsi = (dex+arg)/denom
        if(n.eq.1) go to 520
        if(dabs(vsi/vs(i)).gt.cutoff) ii=1
520       vs(i) = vs(i) + vsi
530       continue
      if(ii.ne.0.or.n.eq.1) go to 510
      vpre = 4.*reorg(l)*rlamb/beta
      rpre = (reorg(l)/rlamb)/tan(rlamb*beta/2.)
      e0(l) = ev(l) - reorg(l)
      do 60 i=1,ntime
        rlambt = rlamb*toverh(i)
        damp = 1. - exp(-rlambt) - rlambt
        rdamp = -rpre*damp + vpre*vs(i)
60        cdamp(l,i) = cexp(-rdamp-ci*reorg(l)*damp/rlamb)
c
c       Now undamped oscillators
c
80              do i=1,2
                  call simpov(l,i,delth,ntime,wg,delta,covlp,ceiwt)
            e0(l) = e0(l) - 0.5*wg(i)*delta(l,i)**2
       end do
       write(31,*) ' e0 = ', e0(l), ' cm-1 in state ', l
c
c    Set up the time integrals
c
      do i=1,ntime
        cat(l,i)=u(l)**2*cexp(-ci*(e0(l)+reorg(l))*toverh(i))
     1             *cdamp(l,i)
      end do
100   continue
c
c       Set up inhomogeneous broadening
c
        close(unit=31)
    xfreq(1) = alow
    xinc = (ahigh-alow)/999.
```

```
      do 166 k=2,1000
 166      xfreq(k) = xfreq(k-1) + xinc
      pfunc(1) = 0.
      do 605 i=2,501
 605     pfunc(i) = pfunc(i-1) + xinc
      if(sig.eq.0.) go to 620
      deno = 2.*sig**2
      do 610 i=1,501
 610      pfunc(i) = exp(-pfunc(i)**2/deno)
c
c     Loop over all Raman lines to calculate. ceiwt is product of overlaps.
c
 620  do 288 j=1,nline
        do 288 n1=0,2
        do 288 n2=0,2
          ei = n1*wg(1) + n2*wg(2)
          wt = exp(-ei*beta)/part
                    do k=1,ntime
             do jj=1,nstate
                                ceiwt(jj,k) = cat(jj,k)
                end do
                            end do
           kk1 = nquanta(j,1)+1
           kk2 = nquanta(j,2)+1
           do l=1,ntime
             do jj=1,nstate
                ceiwt(jj,l)=ceiwt(jj,l)*covlp(jj,1,n1+1,kk1,l)
     1             *covlp(jj,2,n2+1,kk2,l)
                end do
             end do
c
c     Loop over 1000 excitation frequencies
c
                    do 180 k=1,1000
             do jj=1,nstate
                                csum(jj)=0.5*ceiwt(jj,1)
                end do
                            cinc = cexp(ci*(ei+xfreq(k))*delth)
                            cold = (1.,0.)
c
c     Do time integral by simple sum (rectangle rule)
c
                            do 170 l=2,ntime
                                    cold = cold*cinc
```

```
            do 170 jj=1,nstate
 170                              csum(jj) = csum(jj) + cold*ceiwt(jj,l)
          csigmaz = (0.,0.)
          csigmax = (0.,0.)
          do jj=1,nstate
            if(ipol(jj).eq.0) csigmaz = csigmaz + csum(jj)
            if(ipol(jj).ne.0) csigmax = csigmax + csum(jj)
            end do
c
c     Calculate parallel and perpendicular cross sections (k-th excitation freq.,
c           j-th Raman mode)
c
            zx = real(csigmaz*conjg(csigmax)+csigmax*conjg(csigmaz))
            zz = csigmaz*conjg(csigmaz)
            xx = csigmax*conjg(csigmax)
            rrper(k,j) = rrper(k,j) + wt*(zz + xx - zx)
 180          rrpar(k,j) = rrpar(k,j) + wt*(3.*zz + 8.*xx + 2.*zx)
 288               continue
c
c     Convolve with Gaussian inhomogeneous distribution
c
      do 700 i=1,nline
                  do j=1,1000
                        ffunc(j) = rrpar(j,i)
                  end do
         call convl(ffunc,pfunc,gfunc,1000,501,sig)
         do j=1,1000
            rrpar(j,i) = gfunc(j)
            end do
         do j=1,1000
                        ffunc(j) = rrper(j,i)
                  end do
         call convl(ffunc,pfunc,gfunc,1000,501,sig)
         do j=1,1000
            rrper(j,i) = gfunc(j)
            end do
 700      continue
c
c     Print out profiles
c
      do k=1,ngroup
         do j=1,1000
            addper(j) = 0.
            addpar(j) = 0.
```

```
            end do
          do i=k,nline
                  do j=1,1000
            if(igroup(i).eq.k) addper(j) = rrper(j,i) + addper(j)
            if(igroup(i).eq.k) addpar(j) = rrpar(j,i) + addpar(j)
                        end do
      end do
         do j=1,1000
            rrper(j,k) = addper(j)
            rrpar(j,k) = addpar(j)
            end do
         end do
      do 350 i=1,ngroup
                  open(unit=31+i,name=prof//numb(i)//ext)
         do j=1,1000
            xsval = pre*0.25*(rrpar(j,i)+rrper(j,i))*xfreq(j)
     1           *(xfreq(j)-rashift(i))**3
            write(31+i,341) xfreq(j),1.e8*xsval,
     1             rrper(j,i)/rrpar(j,i)
            end do
  341     format(1x,f11.3,5x,e11.4,5x,e11.4)
  350     close(unit=31+i)
c
c     Calculate absorption spectrum
c
  352  pre2 = 5.745e-3*1.e-3*delt/refrac
      do 450 n1=0,2
      do 450 n2=0,2
      ei = n1*wg(1) + n2*wg(2)
      wt = exp(-ei*beta)/part
           do i=1,ntime
                  do j=1,nstate
                        ceiwt(j,i) = cat(j,i)*(ipol(j)+1)
                        end do
                  end do
                  do l=1,ntime
           do jj=1,nstate
                     ceiwt(jj,l) = ceiwt(jj,l)*covlp(jj,1,n1+1,1,l)
     1              *covlp(jj,2,n2+1,1,l)
             end do
                    end do
      do 450 k=1,1000
         csumm = (0.,0.)
         do jj=1,nstate
```

```
                    csumm = csumm+ceiwt(jj,1)
          end do
        csumm = csumm/2.
                cinc = cexp(ci*(ei+xfreq(k))*delth)
                cold = (1.,0.)
                do l=2,ntime
                        cold = cold*cinc
          ceiw = (0.,0.)
          do jj=1,nstate
             ceiw = ceiw + ceiwt(jj,l)
             end do
                        csumm=csumm+cold*ceiw
                        end do
                sigma = abs(real(csumm))*pre2
 450            xs(k) = wt*sigma + xs(k)
     call convl(xs,pfunc,gfunc,1000,501,sig)
     do j=1,1000
                xs(j) = gfunc(j)*xfreq(j)
                end do
     open(unit=31,name='absorp.txt')
     do i=1,1000
                write (31,470) xfreq(i),xs(i)
        end do
 470  format(2f21.14)
     close(unit=31)
c
c     Calculate emission spectrum
c
     xfreq(1) = elow
     xs(1) = 0.
     do k=2,1000
       xs(k) = 0.
       xfreq(k) = xfreq(k-1) + xinc
     end do
     do 650 j=1,2
     do i=1,ntime
       cat(j,i)=cexp(ci*(e0(j)-reorg(j))*toverh(i))
    1    *cdamp(j,i)
        end do
     do 650 n1=0,2
     do 650 n2=0,2
     ei = n1*wg(1) + n2*wg(2)
     wt = exp(-(ei+e0(j)-e0(1))*beta)/part
     do l=1,ntime
```

```
      ceiwt(j,l) = cat(j,l)*covlp(j,1,n1+1,1,l)
     1    *covlp(j,2,n2+1,1,l)
      end do
     do 650 k=1,1000
        csumm = ceiwt(j,1)/2.
                cinc = cexp(ci*(ei-xfreq(k))*delth)
                cold = (1.,0.)
                do l=2,ntime
                        cold = cold*cinc
           ceiw = ceiwt(j,l)
                        csumm=csumm+cold*ceiw
                        end do
                sigma = abs(real(csumm))
 650      xs(k) = wt*sigma + xs(k)
     call convl(xs,pfunc,gfunc,1000,501,sig)
     emax = 0.
     do j=1,1000
                xs(j) = gfunc(j)*xfreq(j)**3
        if(xs(j).gt.emax) emax = xs(j)
                end do
     open(unit=31,name='emiss.txt')
     do i=1,1000
                write (31,470) xfreq(i),xs(i)/emax
        end do
     close(unit=31)
     stop
     end
c
c
     subroutine convl(f,p,g,nf,np,sig)
c
c     calculates the convolution of f with p and returns result in g
c
     dimension f(nf),p(np),g(nf)
c
     if(sig.eq.0.) go to 500
     pmult = p(1)
     sum = pmult
     do 100 i=1,nf
 100      g(i) = f(i)*pmult
     do 300 j=1,np-1
        pmult = p(j+1)
        if(pmult.lt.1.e-5) go to 350
        do 200 k=1,nf
```

```
      kmj = k - j
      if(kmj.gt.0) g(k)=g(k)+pmult*f(kmj)
      kpj = k + j
200    if(kpj.le.nf) g(k)=g(k)+pmult*f(kpj)
300      sum = sum + 2.*pmult
350  do 400 i=1,nf
400      g(i) = g(i)/sum
     return
500  do 510 i=1,nf
510      g(i) = f(i)
     return
     end
c
c
     subroutine simpov(is,n,delth,ntime,wg,delta,covlp,ceiwt)
c
c    Calculates time-dependent overlap for mode with equal ground and
c    excited state frequency
c
     implicit complex (c)
     dimension wg(2),delta(10,2),covlp(10,2,3,3,5000),ceiwt(10,5000)
     dimension calpha(5000)
     data ci/(0.,1.)/sq2/0.7071/
c
     s = delta(is,n)**2/2.
     d2 = delta(is,n)/2.
          sqrts = -delta(is,n)*sq2
     cinc = cexp(-ci*wg(n)*delth)
     cinc2 = cexp(-ci*wg(n)*delth/2.)
     calpha(1) = ci*sq2
     ceiwt(is,1) = 1./cinc2
     do 10 i=2,ntime
        calpha(i) = calpha(i-1)*cinc2
10       ceiwt(is,i) = ceiwt(is,i-1)*cinc
c
c    Calculate <f|i(t)> for i = 0 to 2 and f = i to i+2
c
     do i=1,ntime
       ce = ceiwt(is,i)
       ce1 = 1. - ce
       do ni = 0,2
         do nf = ni,ni+2
           nfi = nf+ni
           kstar = nfi/2
```

```
          cov = (0.,0.)
          do k=0,kstar
            cov=cov+(fact(2*k)/fact(k))*eta(nf,ni,k)
     1           *cherm(nfi-2*k,-d2*ce1/calpha(i))
          end do
          cov = cov*cexp(-s*ce1)*calpha(i)**nfi
          cov = cov/sqrt(fact(nf)*fact(ni)*2.**nfi)
          covlp(is,n,ni+1,nf-ni+1,i) = cov
        end do
      end do
    end do
    return
    end
c
c
c
    function fact(n)
c
    rn = float(n)
    fact = 1.
    if(n.le.1) return
    do i=2,n
       fact = fact*i
       end do
    return
    end
c
c
c
    function eta(jj,ii,kk)
c
    eta = 0.
    do i=1,2*kk+1
       iq = i-1
       eta = eta + comb(jj,2*kk-iq)*comb(ii,iq)*(-1)**iq
       end do
    return
    end
c
c
c
    function comb(m,l)
c
    if(l.gt.m) comb = 0.
```

```
      if(l.le.m) comb = fact(m)/(fact(l)*fact(m-l))
      return
      end
c
c
c
      function cherm(n,carg)
c
      implicit complex (c)
c
      cherm = (1.,0.)
      if(n.eq.1) cherm = 2.*carg
      if(n.eq.2) cherm = 4.*carg**2 - 2.
      if(n.eq.3) cherm = 8.*carg**3 - 12.*carg
      if(n.eq.4) cherm = 16.*carg**4 - 48.*carg**2 + 12.
      if(n.eq.5) cherm = 32.*carg**5 - 160.*carg**3 + 120.*carg
      if(n.eq.6) cherm=64.*carg**6-480.*carg**4+720.*carg**2-120.
      if(n.gt.6.or.n.lt.0) print *,' Hermite polynomial out of range'
      return
      end
c
```

## Appendix IV – Sample Input File for Fortran Code

Sample input file (dashed lines are comments not part of file)

6,2,2,5000

- # excited states, # phonon modes, # Raman lines, # time steps (leave at 5000)

390.,1.e-8,298.

- inhomogeneous broadening standard deviation ($cm^{-1}$), Brownian oscillator cutoff (leave at $10^{-8}$), temperature (K)

17900.,250.,0.01,1.43,1
18000.,250.,0.01,1.43,0
18950.,250.,0.01,0.82,1
19150.,250.,0.01,0.82,0
21200.,700.,0.01,1.5,0
22300.,3800.,0.01,5.1,0

- For each excited state: absorption maximum ($cm^{-1}$), homogeneous HWHM ($cm^{-1}$), Brownian oscillator lineshape parameter (normally leave at 0.01), transition dipole moment (Å), polarization (1 for xy, 0 for z)

15000.,27000.,13000.,0.3,1.49

- low and high range for absorption and RREP calcs ($cm^{-1}$), low range for emission calc ($cm^{-1}$), solvent refractive index

205.,0.35,0.35,0.35,0.35,2.5,0.
207.,0.,0.,0.,0.,0.,0.

- For each phonon mode: frequency ($cm^{-1}$), $\Delta$ in each excited state

1 0 1
2 0 2

- For each Raman line: # quanta excited in each phonon mode, which Raman line that transition contributes to

Output files

absorp.txt: two columns, wavenumber and absorption cross-section
prof0x.txt: for Raman line "x", three columns: wavenumber, Raman cross-section ($x10^8$), depolarization ratio
emiss.txt: two columns, wavenumber and normalized emission spectrum